ISSN 0915-633X

NATIONAL INSTITUTE FOR FUSION SCIENCE

Design Scalings and Optimizations for Super-Conducting Large Helical Devices

K. Yamazaki, O. Motojima, M. Asao, M. Fujiwara and A. Iiyoshi

(Received – Apr. 19, 1990)

NIFS-30 May 1990

RESEARCH REPORT
NIFS Series

NAGOYA, JAPAN

DESIGN SCALINGS AND OPTIMIZATIONS FOR SUPER-CONDUCTING LARGE HELICAL DEVICES

K. YAMAZAKI, O. MOTOJIMA, M. ASAO, M. FUJIWARA, A. IIYOSHI

National Institute for Fusion Science,
Chikusa-ku, Nagoya 464-01,JAPAN

ABSTRACT

Scalings of plasma configurations and engineering device parameters for ℓ=2 helical systems with continuous coils are derived from a wide range of computations. Using these scalings, typical optimized designs of heliotron/torsatron experimental devices with NbTi superconducting (SC) coils are obtained after maximizing a fusion product $n\tau T$ within both physics and engineering constraints.

Optimization studies have been carried out for the next-generation Large Helical Device (LHD) having a major radius of $\sim$ 4 m and magnetic field of $\sim$ 4 Tesla, in which to demonstrate a divertor concept is one of key experiments. These studies clarified that higher γ_c (helical coil pitch parameter) configurations ($\gamma_c \gtrsim$ 1.25) with a larger plasma minor radius are not acceptable from the requirement of the clean divertor configuration. More compact lower-m systems ($m \lesssim$ 8) are bounded by the equilibrium beta limit of the plasma and the stability limit of the SC coil current due to higher maximum magnetic field strength. Larger-aspect-ratio larger-m systems ($m \gtrsim$ 12, $\gamma_c \sim$1.2-1.3) with better neoclassical confinement properties are not effective because of a lower stability beta and a narrower clearance between the divertor layer and the wall. The divertor clearance becomes more severe in normal-conducting (NC) designs than in SC systems, and more than 5-second plasma operations are not possible.

An ℓ=2/m=10/γ=1.2 SC system is found as one of optimized high $n\tau T$ configurations for 4m/4T next-generation experiments with respect to the high-beta requirement, the clean divertor installation, the SC coil engineering and the cost optimization.

KEYWORDS: helical system, superconducting device, system optimization analysis

I. INTRODUCTION

Helical systems[1,2] have distinct advantages in performing steady-state operations without plasma current disruptions in contrast to tokamak systems. Confinement properties of these helical systems are found equivalent to those of tokamak configurations having the same minor radius, and in the last several years three next-generation large experiments have been proposed and designed[3–5]. For designing these devices, engineering optimizations as well as physics optimizations are required. As for tokamak systems, a lot of system analyses have already been carried out, however, there are a few studies on helical systems[6–8]. Especially, a design of helical coils is critical in meeting several physics requirements and in simplifying a device system, because one of major disadvantages of these helical systems is the complicated fabrication and installation of helical coils. Another demerit of the helical system is that the confinement of the helical system is still on the level of the tokamak L-mode as indicated by the so-called "LHD scaling[9]". Without confinement improvements from this empirical scaling, an attractive compact helical reactor may not be realized.

For optimizing the neoclassical confinement in the core region, modular-type coil systems such as the Wendelstein stellarator[4] are effective, as well as for the easy maintenance of superconducting (SC) coils. In these modular coil systems, the fragility of magnetic surfaces is a concern, especially on the edge region. A natural "clean" in-situ divertor configuration is not realized. On the other hand, continuous coil systems such as the Heliotron/Torsatron devices[3,5] are possibly available for controlling the anomalous edge transport by using the clean divertor configurations with high-edge magnetic shear, which is most likely to realize the confinement improvement as found in tokamak H-mode operations. Moreover, to demonstrate these clean divertor configurations is one of key issues for next-generation large helical experiments. The difficulty in fabricating the continuous coil system can be removed by the research and development of demountable SC coil joints. Especially, an enough clearance between the SC coil and the plasma surfaces is required in the design of helical systems, and ℓ=2 heliotron/torsatron configurations with continuous coil system are rather effective for these purposes of the next-generation experiments.

In this paper, New scalings on physics properties and device engineering are derived as a tool for optimizing magnetic configurations of ℓ=2 helical systems with continuous coils. Different from previous works, the present paper deals with empirical scalings and divertor configuration conditions for next-generation experimental machines. A model of optimization study is described in Section 2 relating to magnetic configurations, plasma transport models, divertor conditions, SC coil engineering criteria (stress,

stability and safety) and cost scalings. Typical optimized designs of superconducting heliotron/torsatron systems are presented in Section 3 for the next-generation Large Helical Device (LHD)[3]. The conclusions will be drawn in the final section.

II. MODEL OF OPTIMIZATION ANALYSES

Helical system configurations depends critically on engineering coil designs, especially the allowable coil current density, in addition to physics requirements, which is different from tokamak designs. For optimization of superconducting helical systems, the design consideration is focused on three physics points;

(1) 5 % beta achievement,

(2) maximizing confinement properties,

(3) clean divertor installation,

and on two engineering requirements;

(4) coil current density limits,

(5) device cost estimations.

Among them, the clearance for the divertor configuration (the item (3)) is found a key parameter, as shown later. For the complete optimization, a set of large-scaled computer analyses should be carried out using magnetic-field-line tracing and mapping codes, equilibrium and transport codes, MHD stability codes, technical machine design codes and cost evaluation codes. However, these complicated combinations are not effective in searching for the wide range of configurations. In this paper, new simple various scalings are derived, and an optimization evaluation has been done using these scalings. A scheme of the parameter survey is shown in Fig. 1. For ℓ=2 helical systems, toroidal multipolarity number m, helical coil pitch parameter γ_c ($=ma_c/\ell R_0$; a_c helical coil minor radius and R_0 major radius), central magnetic field strength B_0, coil major radius R_0, and coil current density j_0 are finally determined by the above-mentioned optimization criteria.

As a reference design, a 4m-major-radius / 4T-magnetic-field device is adopted, which is a presently proposed Japanese large helical device LHD[3,10–12] in National Institute for Fusion Science. The typical coil geometry and the plasma configurations are shown in Fig.2. The winding law of helical field coils (HFC) is given by

$$\theta = \frac{m}{\ell} phi + \alpha^* \sin(\frac{m}{\ell}\phi),$$

where α^* is a pitch modulation parameter. To hold flexible and safe operations, the helical coil is divided into multi-layer coils. Three pairs of poloidal field coils (PFC) are used

for shifting, shaping the plasma column and eliminating an induced one-turn voltage. A dumbel-type cross-section of the vacuum vessel is considered to keep the divertor geometry. In the optimization study, the clearance between the divertor and the coil, Δ_{dc}, is an important parameter. Most of parameters are normalized to this m=10/R_0=4m/B_0=4T system. Scalings of magnetic configurations, plasma confinement times and engineering design criteria are described below in turn.

II-1 Scalings of magnetic configurations and Beta conditions

For ℓ=2 helical systems, the magnetic configuration strongly depends on a toroidal multipolarity number m and a helical coil pitch parameter γ_c, and several analytical formula[1]3 for magnetic configuration properties have been already reported. Instead of these analytic and qualitative formula, more realistic and more rigorous formula calculated with finite-sized coils are required for designing the Large Helical Device. For this purpose we used magnetic field tracing code HSD (Helical System Design code) with multi-filament coil models, and calculated magnetic properties for various configurations;

$$\ell = 2, \quad 8 \leqq m \leqq 12, \quad 1.1 \leqq \gamma_c \leqq 1.4,$$

$$R_0 = 4m, \quad -0.025 \leqq \Delta_{ax}/R_0 \leqq 0.$$

Here, we adopted the following input parameters for calculations; ℓ (poloidal multipolarity), m (toroidal multipolarity), γ_c (helical pitch parameter), α^*(helical pitch modulation parameters), R_0(major radius of helical coil) and Δ_{ax} (plasma axis shift). The adopted model of helical coil location and cross-section is shown in Fig.2. The currents of three-pair poloidal coils are determined to adjust axis position, to shape plasma cross-section and to minimize leakage magnetic field far from the torus. Using calculated results and minimizing standard derivaties, the following formula are obtained for the plasma minor radius a_p normalized by the coil minor radius a_c(Fig.3(a)), the minimum inward radius of vertically elongated plasma surface a_{min} (Fig.3(b)), the central rotational transform ι_0 (Fig.3(c)), the surface rotational transform ι_a (Fig.3(d)), and the helical magnetic ripple amplitude at surface ϵ_H (Fig.3(e)):

$$\frac{a_p}{a_c} = 0.54\left(\frac{m}{10}\right)^{0.17}\left[\frac{\gamma_c - 0.9 - 0.44\delta}{0.3}\right]^{0.51} \tag{1}$$

$$\frac{a_{min}}{a_c} = 0.46\left[1. + 0.28\delta\left(\frac{m}{10}\right)^{4.3}\right]\left[\frac{\gamma_c - 0.9}{0.3}\right]^{0.70} \tag{2}$$

$$\frac{\iota_0}{m} = 0.051(1. + 1.5\delta)\left[\frac{1.6 - \gamma_c}{0.4}\right]^{0.70}\left[\frac{0.3}{\gamma_c - 0.9}\right]^{0.95} \tag{3}$$

$$\frac{\iota_a}{m} = \frac{\iota_0}{m} + 0.042(\frac{m}{10})(1. - 4.75\delta)[\frac{\gamma_c - 0.9}{0.3}]^{0.07} \tag{4}$$

$$\epsilon_H = 0.17(\frac{m}{10})^{0.05}[\frac{\gamma_c - 0.9 - 0.29\delta(m/10)}{0.3}]^{0.95} \tag{5}$$

$$\delta \equiv \Delta_{ax}/a_c.$$

Here, to hold closed magnetic surfaces as a plasma confinement region, γ_c should be greater than ~ 0.9 as shown in Ref 13, which is taken into account for choosing these scalings. Resultant standard derivatives and errors with respect to these formula are summarized in Table 1.

For the configuration of helical systems, equilibrium beta limit is estimated by

$$\beta_{eq} = 0.5\frac{\iota_a^2}{A_p}. \tag{6}$$

According to the detailed MHD analysis[12], a 5% stability limit for ℓ=2 systems is roughly described by

$$A_p \lesssim 8. \tag{7}$$

where, A_p is a plasma aspect ratio ($A_p = (R_0 - \Delta_{ax})/a_c$).

Beta conditions are described by the above two equations, and transport estimations shown in a next section are performed using Eqs.(1)$\sim$(5).

II-2 Plasma confinement models

In order to forecast a parameter space of presently proposed large helical systems, a neoclassical ripple transport with proper ambipolar electric field, and an empirical scaling for helical systems are considered. Attainable plasma parameters such as confinement time τ(s), plasma average temperature T(keV), fusion products $nT\tau(10^{20}\mathrm{m}^{-3}\mathrm{keV}\cdot\mathrm{s})$ and plasma beta values $\beta(\%)$ are obtained using input parameters such as a plasma major radius R(m), a plasma minor radius a_p(m), magnetic field strength B(T), absorbed heating input power P(MW) and plasma average density $n(10^{20}\mathrm{m}^{-3})$. The plasma radius, rotational transform, helical ripple percentage etc. are estimated from the scalings mentioned in the previous section.

The transport scalings for estimating τ and T are as follows:

(i)Neoclassical model[14,15]

Plateau regime ($n \geqq n_1$)

$$\tau_{PL} = 1.35P^{-0.6}n^{0.6}B^{0.8}Ra_p^2 < \iota >^{0.4} \tag{8}$$

$$T_{PL} = 1.36 P^{0.4} n^{-0.4} B^{0.8} < \iota >^{0.4} \tag{9}$$

Ripple ion root ($n_1 \geqq n \geqq n_2$)

$$\tau_{RI} = 0.24 P^{-7/9} n B^{4/9} R^{11/9} a_p^2 < \epsilon_H >^{-1/3} \tag{10}$$

$$T_{RI} = 0.26 P^{2/9} B^{4/9} R^{2/9} < \epsilon_H >^{-1/3} \tag{11}$$

Ripple electron root ($n_2 \geqq n$)

$$\tau_{RE} = 1.1 \cdot 10^{-5} P^{1/3} n^{-1} B^{2/3} R^{7/3} a_p^{-2} \tag{12}$$

$$T_{RE} = 1.2 \cdot 10^{-5} P^{4/3} n^{-2} B^{2/3} R^{4/3} a_p^{-4} \tag{13}$$

where characteristic densities for transport regime are given by

$$n_1 = 75.0 P^{0.44} B^{0.89} R^{-5/9} < \iota >< \epsilon_H >^{5/6} \tag{14}$$

$$n_2 = 6.8 \cdot 10^{-3} P^{5/9} B^{1/9} R^{5/9} a_p^{-2} < \epsilon_H >^{1/6}, \tag{15}$$

and average values estimated at a radius of $\sim a_p/\sqrt{2}$ are assumed as,

$$< \iota >= (\iota_0 + \iota_a)/2,$$

$$< \epsilon_H >= \epsilon_H/2.$$

Since the helical ripple transport dominates near the half radius of the plasma column, the coefficients of these global confinement scalings are adjusted after comparing the more detailed calculations[16].

(ii) Empirical scalings

The following so-called LHD scalings[9] are used for empirical predictions.

$$\tau_{EMP} = 0.17 f_{EMP} P^{-0.58} n^{0.69} B^{0.84} R^{0.75} a_p^{2.0} \tag{16}$$

$$T_{EMP} = 0.18 f_{EMP} P^{0.42} n^{-0.31} B^{0.84} R^{-0.25}, \tag{17}$$

Here, an improvement factor of confinement f_{EMP} is introduced. According to most of the above confinement scalings, higher plasma density leads to the improvement of confinement, however the achievable density is limited by the radiation cooling and so on. The experimentally obtained density limit scaling[9] is;

$$n_c = 0.25 (\frac{PB}{a_p^2 R})^{0.5}. \tag{18}$$

In most of optimization studies, $n\tau T$ values are maximized for the empirical confinement scaling at the empirical critical density.

II-3 Divertor Configuration condition

For making in-situ divertor configurations, it is necessary to keep a clearance between the divertor layer and the wall. The distance between them is determined by the coil size, namely the global coil current density j_0, the central magnetic field strength B_0 and the major radius R_0. The distance Δ_{dc} is calculated and summarized in Fig.4(a) in the case of standard helical coil winding law without coil pitch modulations. This curve is approximated by the formula,

$$\Delta_{dc}(m) = (0.14 + 0.28\frac{\Delta_{ax}}{R_0})\frac{R_0}{4}[1.5(\frac{j_0}{40}\frac{R_0}{B_0}\frac{10}{m})^{1.0}(\frac{1.2}{\gamma_c})^{3.5} - 0.5]^{0.6} \tag{19}$$

where, in the case of pitch-modulated helical coil, the coefficient should be modified to $0.14 + 0.28\Delta_{ax}/R_0 + 0.2\alpha^*$. This clearance is critically determined by the coil pitch parameter γ_c and the pitch modulation α^*.

II-4 Coil Engineering Parameters

Different from magnetic surface properties mentioned above, the engineering SC design critically depends on the coil and machine size. Especially, the maximum field strength on the coil conductor, therefore, the permissible SC coil current density and the plasma-wall designs are determined by the machine size and the magnetic field strength.

Using parameters of R_0 (major coil radius), B_0 (magnetic field at coil center) and j_0 (helical coil current density), we can obtain coil parameters such as the total coil current I_c(AT), the coil cross-sectional area S_c(m^2), the coil length l_c, and the global coil volume V_c(m^3):

$$I_c = \frac{2\pi R_0 B_0}{\mu_0 m} \tag{20}$$

$$S_c = \frac{I_c}{j_0} \tag{21}$$

$$l_c = 2\pi R_0 \ell\sqrt{1+\gamma_c^2} \tag{22}$$

$$V_c = l_c S_c = \frac{(4\pi)^2}{\mu_0}\frac{\ell B_0 R_0^2}{m j_0}\sqrt{1+\gamma_c^2} \tag{23}$$

The inductance of helical coils can be estimated from the combination model of m-turn poloidal coils and ℓ-turn toroidal coils.

$$L_c = f_{corr}\mu_0 R_0[m^2(1-\sqrt{1-(\epsilon_c)^2}) + \ell^2(\ln(\frac{8}{\epsilon_c}) - 2)] \tag{24}$$

where,

$$\epsilon_c \equiv \frac{a_c}{R_0}$$

The correction factor f_{corr} of this inductance is found $\sim$1.4 by means of real computations. Different from tokamak configurations, the poloidal component of magnetic energy of the helical system is the same order of the toroidal component, therefore the minimization of magnetic energy is important by means of poloidal coil optimization. The total magnetic energy added by poloidal coils is reduced to typically $\sim$ 80 % of this value, when the leakage magnetic flux outside the torus is minimized.

Using the coil magnetic energy

$$E_{mag} = \frac{1}{2}L_c I_c^2, \tag{25}$$

the electromagnetic force F is calculated by

$$F = \nabla E_{mag} \tag{26}$$

then, hoop and radial forces per unit length, f_R and f_a are

$$f_R = f_{corr}\frac{\mu_0 I_c^2}{4\pi R_c}[\frac{m}{\sqrt{1-(\epsilon_c)^2}} - \frac{\ell}{\epsilon_c}], \tag{27}$$

$$f_a = f_{corr}\frac{\mu_0 I_c^2}{4\pi R_c}[\frac{m}{\epsilon_c}(1 - \frac{1}{\sqrt{1-(\epsilon_c)^2}}) + \ell(\ln(\frac{8}{\epsilon_c}) - 1)]. \tag{28}$$

For the 4m/4T LHD design, the maximum force loaded on the outer leg is higher than 10MN/m.

The maximum magnetic field on coil surface B_{max}, critical SC current density j_0 and the clearance between the divertor separatrix layer and the coil Δ_{dc} are estimated by the scaling laws described bellow .

(i) Maximum field strength in coil

According to the analysis using both 16 × 16 multi-filament-current code (HSD code) and finite-volume-current-element code (MAGN code[17]), the maximum magnetic field strength of the R_0=4.0 m/B_0=4.0 T helical system with ℓ=2 / m=10 is around 8.4 T

in the case of the coil current density of 40 A/mm^2. The ratio between the maximum field on the coil B_{max} and the central field B_0 is determined by the geometrical shape and configuration, and is expressed by the value S_c/R_0^2 for fixed pitch parameter γ_c. If the contribution of the coil filament itself is dominant, the field ratio is $B_{max}/B_0 \propto \sqrt{R_0^2/S_c} \propto \sqrt{j_0 R_0/B_0}$, however, the effect of not only near-by coils but also far coils is important, then the j_0-dependence on the field is relaxed. The computer analysis reveals that the highest field is created on the inner board of the outer helical coil in the case of no application of the poloidal field, and the following scaling is obtained (Fig.4(b)).

$$\frac{B_{max}}{B_0} = 2.1(\frac{j_0}{40}\frac{R_0}{B_0})^{0.40}(\frac{10}{m})^{0.42}(\frac{\gamma_c}{1.2})^{0.05} \tag{29}$$

The real maximum field depends slightly on the PFC position and the operation current strength, but within the 5% accuracy the above equation is valid.

(ii) SC critical current

The critical current density[18,19] of standard NbTi conductor is supposed ~1000 A/mm^2 for 8T at the temperature $\theta = 4.2°$ K, and is scaled as

$$J_{crit}(A/mm^2) = \quad 7300[1 - \frac{B_{max}}{10.5 + 1.4(4.2-\theta)}]/B_{max}^{(0.27-0.09(4.2-\theta))} \tag{30}$$

The critical current of the real coil is determined by the so-called copper ratio f_{stab}, coil packing factor f_{pack}, temperature margin $\Delta\theta$, design safety margin f_m and so on.

$$j_0 \leqq \quad j_{cr} \equiv f_m f_{pack}\frac{1}{1+f_{stab}} J_{crit}(\theta + \Delta\theta) \tag{31}$$

Typically, for bath-cooling coil system the copper ratio f_{stab} is assumed to be 5.0, and the coil packing ratio f_{pack} including insulations is 0.7 . Considering 50% safety margin f_m and 1° K temperature margin $\Delta\theta$, we obtain

$$j_0(A/mm^2) \quad \leqq 426[1 - \frac{B_{max}}{9.1}]/B_{max}^{0.361} \tag{32}$$

for 4.2 ° K system. The current density of helical coil should be less than 49 and 24 A/mm^2 at 7 and 8T, respectively.

(iii) SC stability condition

The conservative design criterion is so-called fully steady-state cryostability and is described[19] by

$$j_0 \leqq j_{st} \equiv f_{pack}\sqrt{\frac{\eta_{cool} q_r}{\rho_{stab}} \frac{p_{cond}}{A_{cond}} \frac{f_{stab}}{1+f_{stab}}} \tag{33}$$

where, resistivities of copper and aluminum stabilizers ρ_{stab} including magneto-resistive effects for the temperature range of $\theta \leqq$ 10 °K are scaled as

$$\rho_{cu}(\Omega \cdot m) = 1.0 \times 10^{-10}(1 + 0.5 B_{max}) \tag{34}$$

$$\rho_{Al}(\Omega \cdot m) = 3.4 \times 10^{-11}(1 + 0.15 B_{max}) \tag{35}$$

Here, the resistivity of the aluminum stabilizer is used for optimization study. Typically, for bath-cooling coil system the cooling efficiency η_{cool} is assumed 0.6 and heat flux q_r is $3 \cdot 10^3 \mathrm{W/m^2}$ at 4.2 ° K. By decreasing the coil temperature to 1.8 ° K, the super-fluid heat transfer is expected and q_r can be increased to $1\mathrm{x}10^4 \mathrm{W/m^2}$. The ratio of the cross-sectional area to the perimeter A_{cond}/p_{cond} depends on the coil conductor design and for $\sim$ 20-30kA conductors this value is typically $6\mathrm{x}10^{-3}$ m. Then, we can obtain the condition for 4.2-4.4 ° K:

$$j_0(A/mm^2) \leqq \frac{60.0}{\sqrt{1 + 0.15 B_{max}}} \tag{36}$$

For B_{max} = 5 or 8T system, the current density of helical coils should be less than 45 or 40 $\mathrm{A/mm^2}$, respectively.

(iv) SC protection condition

For the safety protection of SC coil system, the temperature rise at the spot area should be lower than the certain level, even if the SC coil is quenched. The condition for this "hot spot" model is described[18,19] by;

$$j_0 \leqq \quad j_{pr} \equiv f_{pack} \frac{f_{stab}}{1+f_{stab}} \sqrt{\frac{U_m V_{max} I_{cond}}{(E_{mag}/N_{block})}} \tag{37}$$

Here, typically, an allowable maximum coil voltage V_{max} is 1 kV, the conductor current I_{cond} is 30 kA, and the total magnetic energy is divided to N_{block} number. The temperature rise from θ_i to θ_m should be less than $\sim$ 100 ° K and the related safety function U_m is;

$$U_m \equiv \int_{\theta_i}^{\theta_m} \gamma_{heat} \frac{C(\theta)}{\rho(\theta)} d\theta \quad \leqq \quad 1 \cdot 10^{17} A^2/s \cdot m^4 \tag{38}$$

Then, we obtain the safety condition

$$j_0(A/mm^2) \quad \leqq \quad \frac{32.0}{\sqrt{E_{mag}(GJ)/N_{block}}} \tag{39}$$

When the 2GJ coil system with 6 separation coil blocks is considered, the current density of 55A/mm^2 is the allowable limit.

(v) Electromagnetic stress

The electromagnetic force on the coil F is proportional to $B_0^2 R_0^2$, and the stress σ_c is roughly estimated from

$$\sigma_c \propto \frac{F}{R_0\sqrt{S_c}} \propto \sqrt{B_0^3 R_0 j_0}.$$

More precisely, using Eqs.(27) and (28) the magnetic stress is estimated by

$$\sigma_c = \frac{|f_R| + |f_a|}{(1-\eta_{cool})\sqrt{f_{pack} S_c}} \tag{40}$$

For standard LHD parameters with m=10,R_0=4m,B_0=4T and $\epsilon_c = 0.24$, the total force per unit length is 12.8 MN/m and coil area S_c is 0.2 m^2, therefore, the coil stress σ is 8.7 kg/mm^2, which is below the permissible level of 10 kg/mm^2. The condition $\sigma_c \leqq$ 10 kg/mm^2 leads to:

$$j_0(A/mm^2) \quad \leqq \frac{1.35 \cdot 10^4}{R_0 B_0^3}. \tag{41}$$

The real stress depends on the support structure, and the more detailed analysis is required for the more precise design instead of these simple optimization scalings.

II-5 Cost-relevant Index

Most expensive component of the experimental helical system is the helical coil and the device cost is roughly estimated from the coil conductor gross volume $V_c \propto R_0^2 B_0 / j_0$. Another simple cost index is the coil magnetic energy $E_{mag} \propto R_0^3 B_0^2$. For present optimization study, the helical coil volume V_c or weight is mainly adopted as a simple cost index. More detailed cost indices composed from those of poloidal coils, vacuum vessel, power supplies and so on are written in Table 2 denoting B_0, R_0, j_0 dependences. The cost is estimated from the summation among the material cost, the fabrication cost, the designing cost, the installation cost and so on. All these decomposed costs are assumed to be proportional to its material cost. The cost of a coil-winding machine is mainly

proportional to the major radius. The weight of poloidal coils is proportional to the PF coil current and the major radius for fixed current density, therefore to $R_0^3 B_0$. The cost of vacuum vessel is estimated by R_0^2 because of the almost constant thickness of the wall for $R_0 = 3 \sim 6$ systems. The cost of the cryostat is $\sim R_0^3$ for the constant stress assumption with the wall thickness proportional to R_0. Each percentage of these component costs is obtained from the real detailed cost evaluations for the 4.0m/4.0T/40A/mm^2 LHD SC machine[10,11], which is different from reactor cost evaluations[20-22].

Typical dependence of LHD device cost on the major radius and the magnetic field strength is shown in Fig.5. The effect of change in the major radius on the cost index is larger than that of changing the magnetic field strength.

III. OPTIMIZATION RESULTS

III-1 Configuration Variations on $m - \gamma_c$ Plane

Using above-mentioned scalings and data base, we carried out the optimization analysis on the basis of the ℓ=2 m=10 γ_c=1.2 reference design with major radius of 4.0 m, magnetic field of 4.0 T and helical coil current density of 40 A/mm^2. The non-dimensional properties for various magnetic configurations are shown on the $m - \gamma_c$ plane in Fig.6. To reduce the plasma aspect ratio A_p for aiming compact configurations, the reduction of the m-number or the increase of the γ_c value is required. On the other hand, the increase in the central or surface rotational transform is attained by increasing m-number and decreasing γ_c value. For the rough choice of magnetic configuration, high equilibrium beta ($\beta_{eq} \gtrsim$ 5%), lower-aspect-ratio and 5% stability condition ($A_p \lesssim 8$) and appropriate central rotational transform requirements ($\iota_0 \gtrsim 0.3$) are taken into account. The shaded region in this figure shows these configuration requirements in the cases of no magnetic axis-shift (Fig.6(a)) and 2.5% axis-shift (Fig.6(b)). The beta limitation determines an allowable range of m-number, and a comparison between the present simple beta scalings and the detailed MHD results[12] is shown in Fig.6(c), which suggests a rough agreement between them. The equilibrium beta condition leads to the lower boundary of m-numbers and the stability beta gives rise to the upper boundary of m-number and the lower boundary of γ_c values. These beta and rotational transform properties slightly depends on the coil size even for the fixed m- and γ_c-values, but in the present optimization study these small effects are neglected. In contrast to these dimensionless constraints, the divertor condition critically depends on the wall and coil

sizes, which determines an upper boundary of γ_c values.

III-2 Comparisons between Normal- and Super-Conducting Designs

A radial build from the plasma surface to the coil is an important parameter for determining the divertor clearance. In the present LHD standard design, the thickness on the stainless-steel coil can is 4.5 cm and the thickness of the vacuum vessel is 3.0 cm. The vacuum thermal insulation layer is 5.0 cm thick, and the thickness of carbon tiles is designed less than 2.5 cm. Then, the total thickness between the coil surface and the first-wall surface Δ_{wc} should be less than 15cm. On the other hand, the gap between the wall surface and the divertor layer Δ_{gap} should be larger than 3.0 cm to keep divertor configurations. Therefore, for a "standard vessel design", the condition

$$\Delta_{dc}(=\Delta_{wc}+\Delta_{gap}) \quad \geqq \quad 18cm \tag{42}$$

is considered. Another design called a "reference vessel design" is more aggressive than this , and the condition

$$\Delta_{dc} \quad \geqq \quad 14cm \tag{43}$$

is adopted for a present optimization constraint by reducing these thickness. As for NC designs, the thermal insulation layer can be removed and these conditions are relaxed as

$$\Delta_{dc} \quad \geqq \quad 9cm. \tag{44}$$

The coil size also has critical effects on the optimization study of helical configurations. The current density of the helical coil determined by the pulse length for normal-conducting (NC) coil systems and by the stability and safety conditions for superconducting (SC) coil systems. The permissible pulse length of the NC conductor is determined mainly by the temperature rise of the conductor and the required scale of the power supply. For LHD parameters, the total equivalent square-pulse length for 20,30 and 40 A/mm^2 with packing factor of $\sim$0.7 are $\sim 15, \sim 7$ and ~ 4 seconds, respectively. On the other hand, the equivalent square-pulse length required for rising and falling the coil current, are 10, 7 and 5 seconds with the voltage forcing rate of $\sim$1.5, respectively. Therefore, more than 5-second flat-top requires roughly less than 20 A/mm^2 gross current density for 4m/4T NC systems. The optimum region for the "reference vessel design" and the 30 A/mm^2 NC coil design making less than $\sim$1 s flat-top time operation is equivalent to the 4m/4T SC design with 40 A/mm^2, as shown in Fig.7. In addition to the difficulty of the long-pulsed operation, the induction of the one-turn voltage due to the pulse operation is a serious problem related to the production of runaway electrons. The deformation of coils due to the temperature rise is also concerned in the NC system.

It is found that when more than 5-second operation time is required for LHD-class devices, it is proper to choose SC devices, instead of NC machines.

III-3 $m - \gamma_c/B_0 - R_0$ optimizations for LHD

For the fixed major radius and the fixed magnetic field strength, the optimum regions are shown on the $m - \gamma_c$ plot in the previous section. Instead of the fixed size model, it is appropriate to reduce the major radius for lower m-number systems and increase it for higher m systems within the fixed cost model. As a simple cost estimation, the model of the constant helical-coil weight is used for a cost index and the following coil-current-density models are taken into account.

The current density of the helical coil for "LHD standard coil design" with $\Delta\theta$ of 1.0°K and f_m of 0.5 is given by Eq.(32). For the present "reference and aggressive coil design" with $\Delta\theta$ of 0.5 $°K and f_m$ of 0.7, the condition is

$$j_0(A/mm^2) \quad \leqq 596[1 - \frac{B_{max}}{9.8}]/B_{max}^{0.315}. \tag{45}$$

Figure 8 shows this maximum current density as a function of maximum magnetic field, as denoted by (i-a) for Eq.(45). Other constraints on the current density relating to the B-field limit (Eqs.(32)), the stability limit (Eq.(36)), the safety limit (Eq.(39)) and the stress limit (Eq.(41)) are also plotted in Fig.8 for the heating power of 20 MW.

For the fixed magnetic field strength of 4.0 Tesla and the constant gross coil volume of 15.7 m^3, optimized parameters of R_0 and j_0 are obtained for each m-number and γ_c value (FIg.9). Other parameters such as Δ_{dc},V_p,j_0,B_{max}, $n_c\tau T_{EMP}$, $n_c\tau T_{RI}$, E_{mag}, C_{dev} and C_{tot} are also drawn on the $m - \gamma_c$ plot, which is obtained by using the "reference coil model" (Eq.(45)). An optimized domain derived from the beta conditions and the reference vessel criterion (Eq.(43)) is shaded. Within these boundaries, the fusion product $n\tau T$ should be maximized. When a maximum $n\tau T$ value is requested with respect to the empirical transport, the γ_c value should be raised to the limit of the divertor clearance. When we wish to improve the neoclassical confinement, the m-number should be increased up to the boundary of the divertor-beta limitation.

Depending on the magnetic field strength, the optimal γ_c for each m-value is obtained. Figure 10 shows changes in various parameters as B_0, R_0, j_0, B_{max}, V_p, n_c,$n_c\tau T_{EMP}$, $n_c\tau T_{RI}$, C_{dev} and C_{tot} for the case of 20 MW heating power. For maximizing $n\tau T$ value with respect to the empirical scaling, the higher B_0 and the smaller γ_c configuration is optimal

for each m-number, as shown in Figs. 10(a) and (d). This optimization is carried out with the constraints of the constant coil volume and the constant divertor clearance. The detailed cost index is higher for the higher-m and larger-R configurations as denoted in Fig.10(e).

Table 3 shows optimized device parameters for each m-number, which are obtained after the full optimization with the procedure of Fig.1 . The beta limitation, the constant divertor clearance Δ_{dc}, the SC current stability conditions and the same total cost index are taken into account. The γ_c values are determined mainly by the beta requirement for each m-number system. The axis shift Δ_{dc} is chosen as

$$\Delta_{ax} \sim \epsilon_c a_c.$$

For the m=14 device the major radius is ~5m and the magnetic field is ~3T. By decreasing m-number, reducing the major radius and increasing the field strength, higher $n\tau T$ values are obtained. On the other hand, the empirical confinement time is maximized on the m=10 system, because the maximum field on the coil conductor for lower m system ($m \leqq 8$) becomes larger than 8.5 T and the allowable current density is reduced substantially. Therefore, the optimum device performance is obtained at $m \sim 10$.

IV. CONCLUSIONS

New scaling formula for physics and engineering designs of ℓ=2 large helical devices are derived, and by using these scalings system optimization studies have been carried out. Physics constraints are (i) the high beta achievement ($\beta \gtrsim$ 5%), (ii) the appropriate clearance between the divertor layer and the coil ($\Delta_{dc} \gtrsim 14 \sim 18$ cm) and (iii) the maximization of the fusion product $n\tau T$, and engineering constraints are (i)SC coil engineering and (ii) the cost estimation .

After optimization studies focusing on divertor and long-pulse experiments, we have reached the following conclusions:

(1) A higher helical-pitch-parameter ($\gamma_c \gtrsim$ 1.3) configuration with a larger plasma minor radius is prohibited from the divertor clearance for next-generation machines. A rather compact lower-m ($m \lesssim$ 8) system is bounded by the equilibrium beta limit and the coil current stability limit related to higher maximum magnetic field strength on the SC coil. A larger-aspect-ratio large-m ($m \gtrsim$ 12) system with good neoclassical confinement is not acceptable because of the lower stability beta and the narrow divertor clearance.

(2) A higher-field smaller-scale system ($B_0 \gtrsim$ 4.5T) suffers from difficulties of the divertor installation and the SC current instability of NbTi conductors. On the other hand, a lower-field larger-scale device ($R_0 \gtrsim$ 5m) is not acceptable due to the lower plasma temperature, the higher electromagnetic stress and the cost constraint.

(3) Normal conductor systems for 4m/4T machines are not allowable because of the difficulty of keeping the appropriate divertor-clearance and the $\gtrsim$ 5-second long-pulsed operation.

(4) An ℓ=2 / m=10 / γ=1.2 system with coil current density of 40 A/mm^2 is found as a optimized higher-beta better-confinement configuration with respect to divertor installations, SC coil engineering requirements and cost optimizations

ACKNOWLEDGMENT

The authors are grateful to all members of LHD Design Group and engineers of Hitachi, Toshiba and Mitsubishi Companies for fruitful discussions. One of authors (M.A.) is on leave from Kobe Steel LTD.

REFERENCES

1. B.A.CARRERAS, G.GRIEGER, J.H.HARRIS, J.L.JOHNSON, and J.F.LYON, "Progress in Stellarator/Heliotron Research: 1981-1986," *Nucl. Fusion,* 28,1613(1988).

2. J.F.LYON, "Near-Term Directions in the World Stellarator Program," *Fusion Technol.,* 17,19(1990).

3. A.IIYOSHI, M.FUJIWARA, O.MOTOJIMA, N.OHYABU, and K.YAMAZAKI, "Design Study for the Large Helical Device," *Fusion Technol.,* 17,169(1990).

4. C.BEIDLER, G.GRIEGER, F.HERRNEGGER, E.HARMEYER, J.KISSLINGER, H.MAASSBERG et al., "Physics and Engineering Design for Wendelstein VII-X," *Fusion Technol.,* 17,148(1990).

5. J.F.LYON, B.A.CARRERAS, N.DOMINGUEZ, L.DRESNER, et al., "Advanced Toroidal Facility II Studies," *Fusion Technol.,* 17,148(1990).

6. R.E.POTOK, H.BECKER, L.BROMBERG, D.R.COHN, N.DIATCHENKO, P.B.ROEMER, J.E.C.WILLIAMS, "Physics and Engineering Constraints for Tokamak Reactors with Helical Coils," *Nucl. Technol. / Fusion,* 4,1314(1983).

7. W.N.G.HITCHON, "Reduced-Aspect-Ratio Stellarator Reactors," *Nucl. Fusion,* 17, 91(1984).

8. J.F.LYON, B.A.CARRERAS, V.E.LYNCH, J.S.TOLLIVER, I.N.SVIATOSLAVSKY, "Compact Torsatron Reactors," *Fusion Technol.,* 15,1401(1989).

9. S.SUDO, Y.TAKEIRI, H.ZUSHI, F.SANO, et al., "Scalings of Energy Confinement and Density Limit in Stellarator/Heliotron Devices," *Nucl. Fusion* , 30,11(1990).

10. O.MOTOJIMA, K.YAMAZAKI, T.MUTOH, Y.TAKEIRI, et al., "Engineering Design Study of the Large SUperconducting Helical Device," *Proc. 15th Int. Symp. Nuclear Fusion,* Utrecht, The Netherlands, September 19-23, 1988, Vol.1, p.402(1988).

11. K.YAMAZAKI, O.MOTOJIMA, S.MORIMOTO, K.NISHIMURA,et al., "Comparative Design Study of Super- vs. Normal-Conducting Large Helical Device," *Proc. 15th*

Int. Symp. Nuclear Fusion, Utrecht, The Netherlands, September 19-23, 1988, Vol.1, p.407(1988).

12. J.TODOROKI, T.KAMIMURA, H.SANUKI, T.AMANO, et al., "MHD and Transport Study of ℓ=2 Heliotron/Torsatron," *Proc.12th Int.Conf. Plasma Physics and Controlled Nuclear Fusion Research,* Niece, France, October 12-19,1988, Vol.2, p.637(1989).

13. D.MARTY, E.K.MASCHKE, J.TOUCHE, C.GOURDON, "Torsatron without Toroidal Field Coils II. Configuration ℓ=2," *Nucl. Fusion,* **12**,367(1972).

14. L.M.KOVRIZHNYKH, "Neoclassical theory of Transport Processes in Toroidal Magnetic Confinement Systems, with emphasis on Non-Axisymmetric Configurations," *Nucl. Fusion* **24**,851(1984).

15. D.D.-M. Ho, and R.M.KULSRUD, "Neoclassical Transport in Stellarators," *Phys. Fluids,* **30**,442(1987).

16. Y.NAKAMURA, and M.WAKATANI, "Transport Simulations of New Stellarator/Heliotron Devices Based on the Neoclassical Ripple Transport associated with an Edge Turbulence," PPLK-R-24, Kyoto University Plasma Physics Laboratory(1988).

17. J.TODOROKI,J., "Magnetic Field Calculation of Finite Size Helical Coils with Rectangular Cross Section," *Kakuyugo Kenkyu,* **57**,318(1987).

18. M.N.WILSON, "Superconducting Magnets," Oxford Science Publications 1983.

19. P.N.HAUBANREICH, M.S.LUBELL, D.N.CORNISH, D.S.BEARD, "Review Paper: Superconducting Magnet for Fusion," *Nucl.Fusion* **22**,1209(1982).

20. J.SHEFFIELD, A.GIBSON, "Cost scaling of Tokamaks," *Nucl. Fusion,* 15,677(1975).

21. W.R.SPEARS, J.A.WESSON, "Scalings of Tokamak Reactor Costs," *Nucl. Fusion,* **20**,1525(1980).

22. S.C.SCHULTE, T.L.WILLKE, J.R.YOUNG, "Fusion Reactor Design Studies - Standard Accounts for Cost Estimates" PNL-2648, Pacific Northwest Laboratory(1978); S.C.SCHULTE, W.E.BICKFORD, C.E.WILLINGHAM, S.K.GHOSE, M.G.WALKER,

"Fusion Reactor Design Studies - Standard Unit Costs and Cost Scaling Rules" PNL-2987, Pacific Northwest Laboratory(1979).

TABLE I: ERRORS OF SCALINGS

Formula	Root-Mean-Square Error (%)	Standard Error (%)
a_p/a_c	4.4	9.9
a_{min}/a_c	6.2	8.9
ι_0/m	0.045	0.79
ι_a/m	0.69	3.5
ϵ_H	4.3	7.3

TABLE II: COST INDEX SCALINGS FOR LARGE HELICAL DEVICES

Items	Device Cost Index (%)	Total Cost Index (%)	Dependence on B_0,R_0,j_0
Helical Coils	47.9	37.9	V_c (Eq.(23))
Winding Machine	4.6	3.6	R_0
Poloidal Coils	20.2	16.0	$R_0^2B_0$
Vacuum Vessel	17.9	14.2	R_0^2
Cryostat	9.4	7.4	R_0^3
(Torus Device Total)	(100.0)	(79.1)	
Control & Plasma Production		3.7	const
Vacuum Exhaust System		2.6	R_0^2
Power Supply & Cooling System		5.3	$R_0^3B_0^2$
Cryogenic System		9.3	$R_0^3B_0^2$
(Auxiliary System Total)		(20.9)	
Total(%)	100.0	100.0	

TABLE III: OPTIMAL DESIGNS FOR EACH m-NUMBER SYSTEM

m-number	$m=$ 8	$m=$ 10	$m=$ 12	$m=$ 14
γ_c	1.15	1.20	1.27	1.35
α^*	0.0	0.0	0.0	0.0
$\beta_{st}(\%)$	$\gtrsim 5\%$	$\gtrsim 5\%$	$\gtrsim 5\%$	$\gtrsim 5\%$
$\beta_{eq}(\%)$	$\sim$5%	>6%	>8%	>10%
Δ_{dc}(m)	0.14	0.14	0.14	0.14
Δ_{ax}/a_c	0.144	0.120	0.105	0.096
A_p	6.35	7.2	7.63	7.84
ι_a/ι_0	0.86/0.41	1.08/0.41	1.29/0.37	1.53/0.30
ϵ_H	0.17	0.17	0.17	0.17
R_0(m)/a_c(m)	3.58/1.03	4.00/0.96	4.47/0.95	4.95/0.95
B_0(T)/B_{max}(T)	4.1/8.6	4.0/8.4	3.5/7.6	3.0/6.9
j_0(A/mm^2)	36.5	40.0	41.0	42.1
$\alpha_{cr} \equiv (j_0/j_{cr})^2$	1.00	0.83	0.34	0.19
$\alpha_{st} \equiv (j_0/j_{st})^2$	0.85	1.00	1.00	1.00
$U_m(10^{17}A^2/s \cdot m^4)$	0.45	0.52	0.45	0.37
σ_c(kg/mm^2)	8.17	8.70	7.60	6.46
R_p(m)/a_p(m)	3.43/0.54	3.88/0.54	4.37/0.57	4.86/0.62
V_p(m^3)	19.8	22.4	28.3	36.8
P(MW)	20	20	20	20
$\overline{n} = \overline{n}_c(10^{20}m^3)$	2.26	2.10	1.75	1.42
τ_{EMP}(s)	0.126	0.129	0.124	0.12
$\overline{T}_{EMP}$(keV)	1.18	1.15	1.06	0.96
$\overline{n}\tau\overline{T}_{EMP}(10^{20}m^3 \cdot$ s $\cdot$ keV)	0.34	0.31	0.23	0.16
τ_{RI}/τ_{EMP}	2.37	2.46	2.59	2.70
V_c(m^3)	17.2(153ton)	15.7 (140 ton)	14.4(128ton)	13.2(117ton)
E_{mag}(GJ)	2.12	2.02	1.64	1.30
C_{dev}	0.98	1.00	1.025	1.05
C_{tot}	1.00	1.00	1.00	1.00

FIGURE CAPTIONS

FIG.1 Scheme of optimization studies with respect to three physics and two engineering constrains.

FIG.2 Geometry of HF and PF coils, vessels and divertor plasma configurations.

FIG.3 Scalings of magnetic configurations.
(a) Plasma radius divided by coil radius,
(b) Minimum inward radius divided by coil radius,
(c) Central rotational transform per one pitch,
(d) Surface rotational transform per one pitch,
(e) Surface helical ripple.

FIG.4 Scalings relevant to coil design parameters.
(a) Minimum distance between coil surface and divertor layer,
(b) Maximum magnetic field strength divided by central magnetic field strength.

FIG.5 Cost indices normalized by that of the m=10/R_0=4m/B_0=4T reference design. Solid and broken lines show total cost and device cost, respectively.
(a) R_0-dependence from the reference design,
(b) B_0-dependence from the reference design.

FIG.6 Magnetic configuration parameters on the $m - \gamma_c$ plot.
(a) no axis-shift case,
(b) 2.5% inward axis-shift case,
(c) Comparison between the present scaling beta values and the exact MHD results (solid curves)of Ref.12 .

FIG.7 Divertor constraints for 4m-4T designs on $m - \gamma_c$ plane.
Broken lines shows equilibrium and stability beta limits of Fig.6(c),
(a) NC design case,
(b) SC design case of 40 A/mm^2 coil current density.
A shaded region denotes permissible designs.

FIG.8 Permissible current density of NbTi SC coil.
(i-a) higher field limit of Eq.(45),
(i-b) higher field limit of Eq.(32),
(ii) stability limit of Eq.(36),
(iii) safety limit of Eq.(39) for $E_{mag} = 2GJ$ and N_{block}=6,
(iv) stress limit of Eq.(41) for $R_0 = 4$m and $B_{max} = 2.4B_0$ case.

FIG.9 Optimization results for 4T case with the same coil-volume constraint of 15.7 m^3.
Dotted lines show equilibrium and stability beta limits.
(a) Major radius R, divertor coil clearance Δ_{dc} (solid lines) and plasma volume V_p (broken line),
(b) Coil current density j_0 (solid line) and maximum magnetic field B_{max} (broken line) on HFC,
(c) Maximum fusion product for empirical scaling $n_cT\tau_{EMP}$ (solid lines), and ripple ion root transport $n_cT\tau_{RI}$ (broken lines) with 20 MW heating power.
(d) Magnetic coil energy E_{mag} (solid line) and cost index of torus device C_{dev} (broken lines) and total system C_{tot} (solid lines)

FIG.10 Optimization results with Δ_{dc}=14cm and V_c=15.7m^3 .
Dotted line shows equilibrium and stability beta limits.
(a) Magnetic field strength B_0 (solid lines) and major radius R (broken lines),
(b) Coil current density j_0 (solid line) and maximum magnetic field B_{max} (broken line) on HFC,
(c) Critical density n_c (solid lines) and plasma volume V_p(broken lines),
(d) Maximum fusion product for empirical scaling $n_cT\tau_{EMP}$ (solid lines), and ripple ion root transport $n_cT\tau_{RI}$ (bar(broken lines),
(e) Cost index of torus device C_{dev} (broken lines), and total system C_{tot} (solid lines).

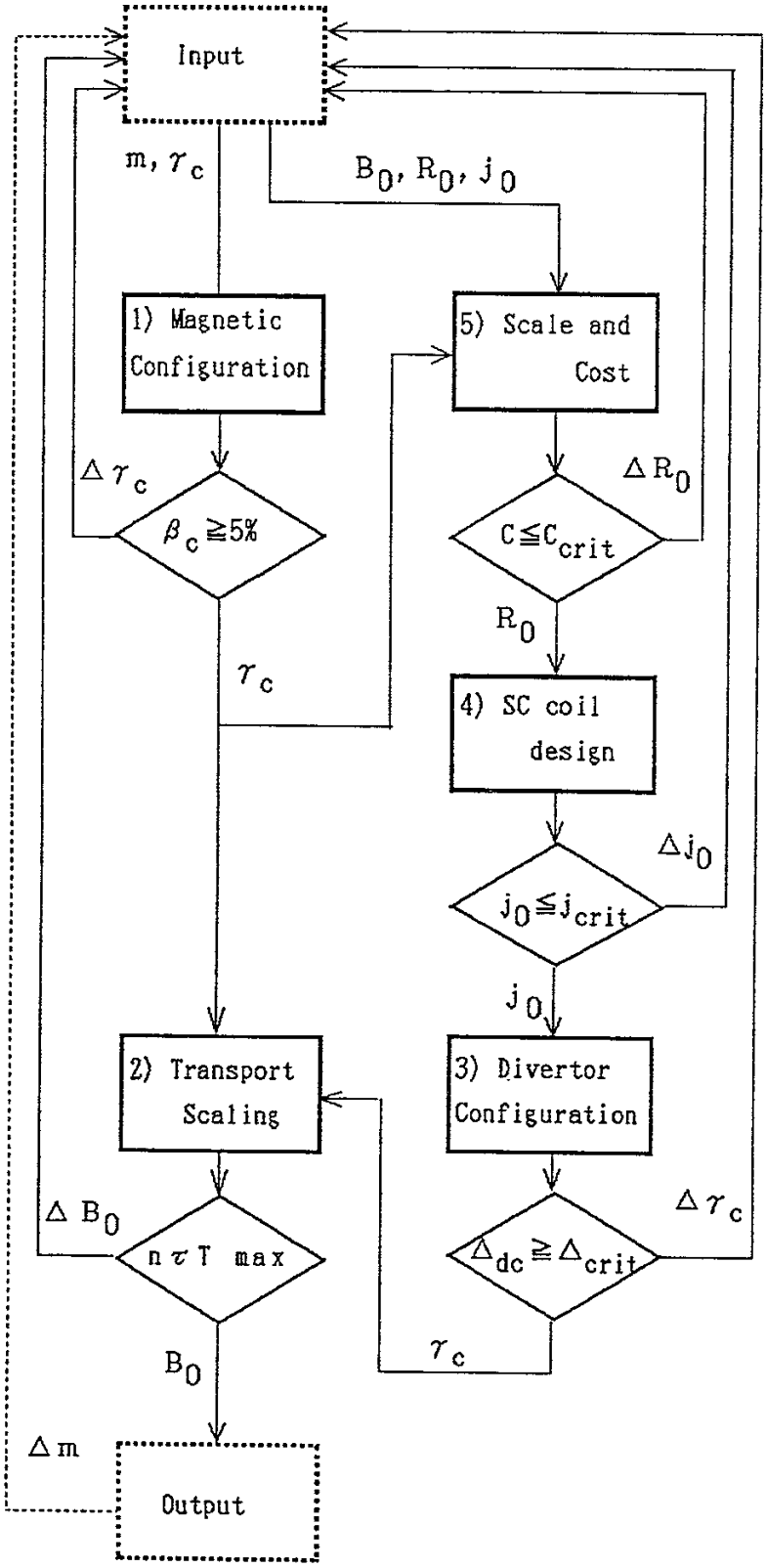
Input
m, τ_c
B_0, R_0, j_0
1) Magnetic Configuration
5) Scale and Cost
$\Delta\tau_c$
$\beta_c \geqq 5\%$
ΔR_0
$C \leqq C_{crit}$
R_0
τ_c
4) SC coil design
Δj_0
$j_0 \leqq j_{crit}$
j_0
2) Transport Scaling
3) Divertor Configuration
ΔB_0
$n\tau T$ max
$\Delta_{dc} \geqq \Delta_{crit}$
$\Delta\tau_c$
τ_c
B_0
Δm
Output

Fig.1

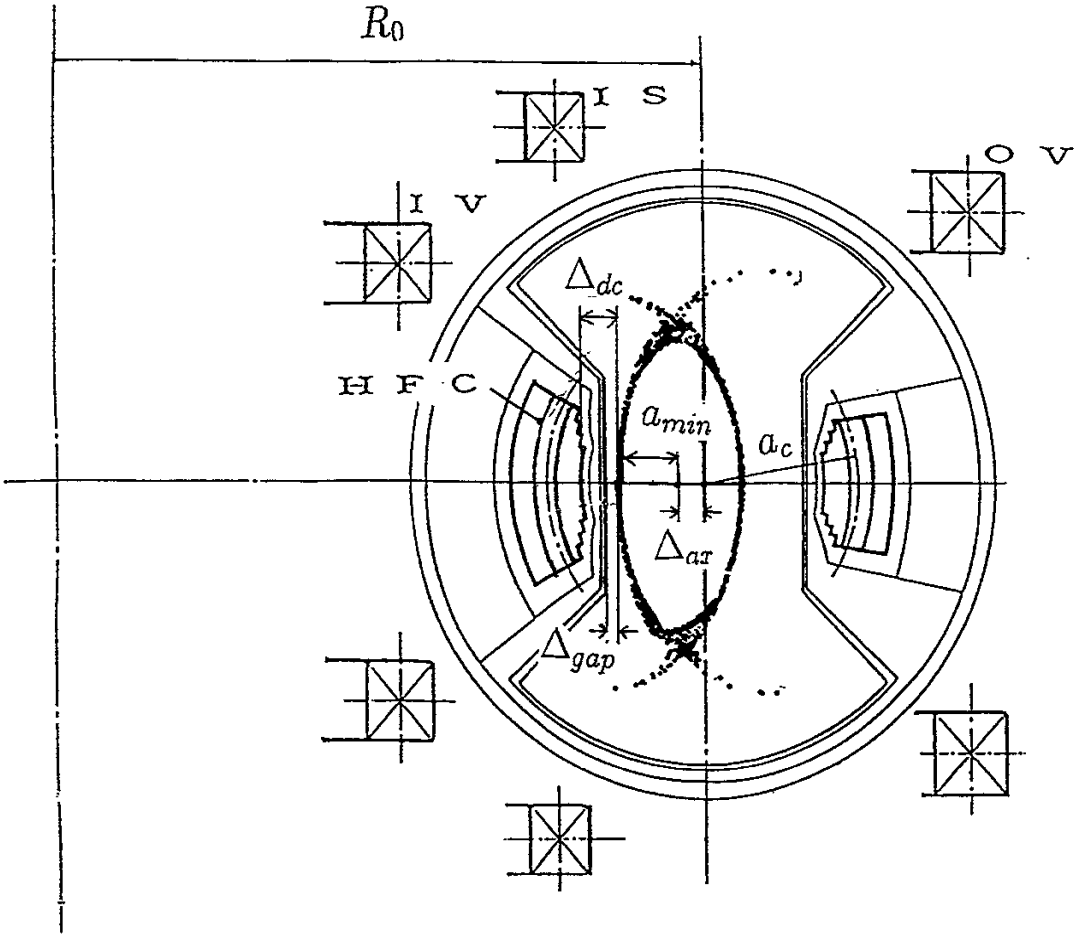

Fig.2

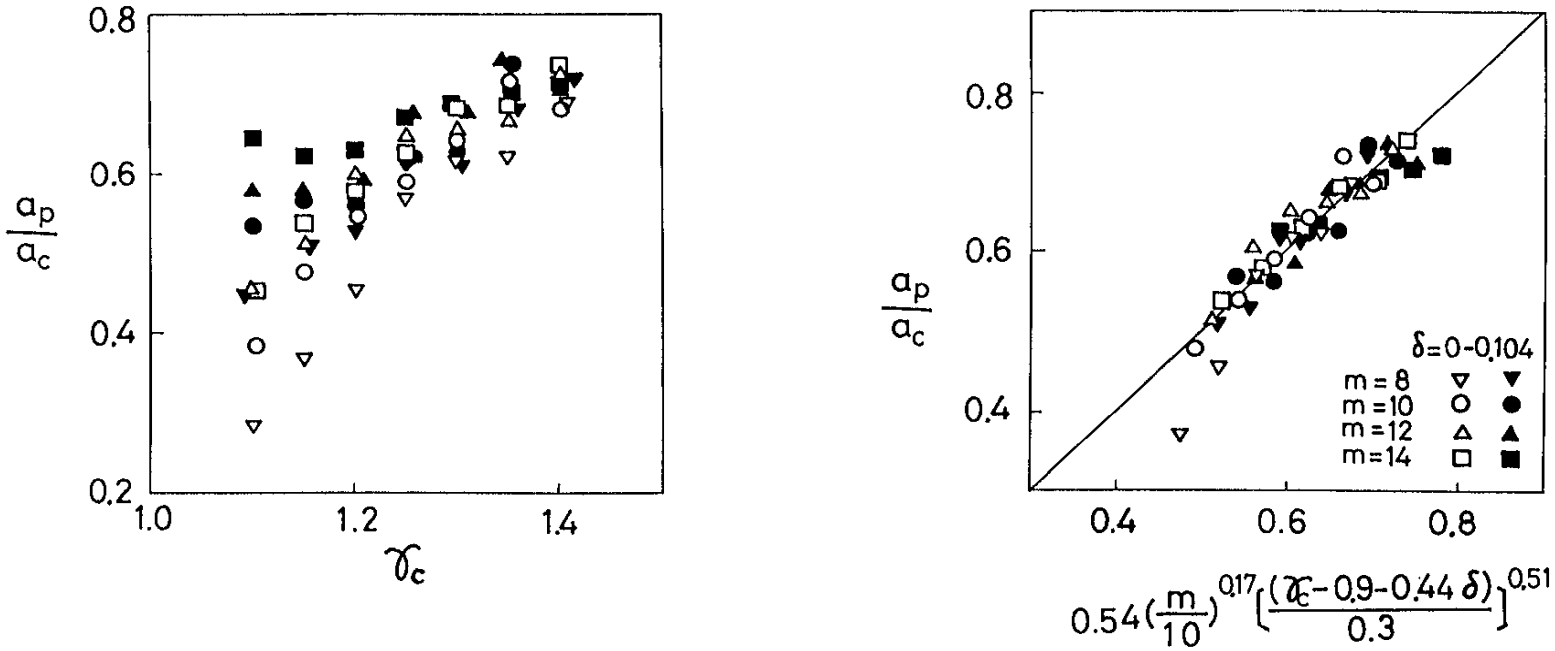
0.8
0.6
0.4
0.2
1.0
1.2
1.4
$\frac{a_p}{a_c}$
γ_c
0.8
0.6
0.4
$\frac{a_p}{a_c}$
δ=0-0.104
m=8
m=10
m=12
m=14
0.4
0.6
0.8
$0.54(\frac{m}{10})^{0.17}[\frac{(\gamma_c-0.9-0.44\,\delta)}{0.3}]^{0.51}$

Fig.3(a)

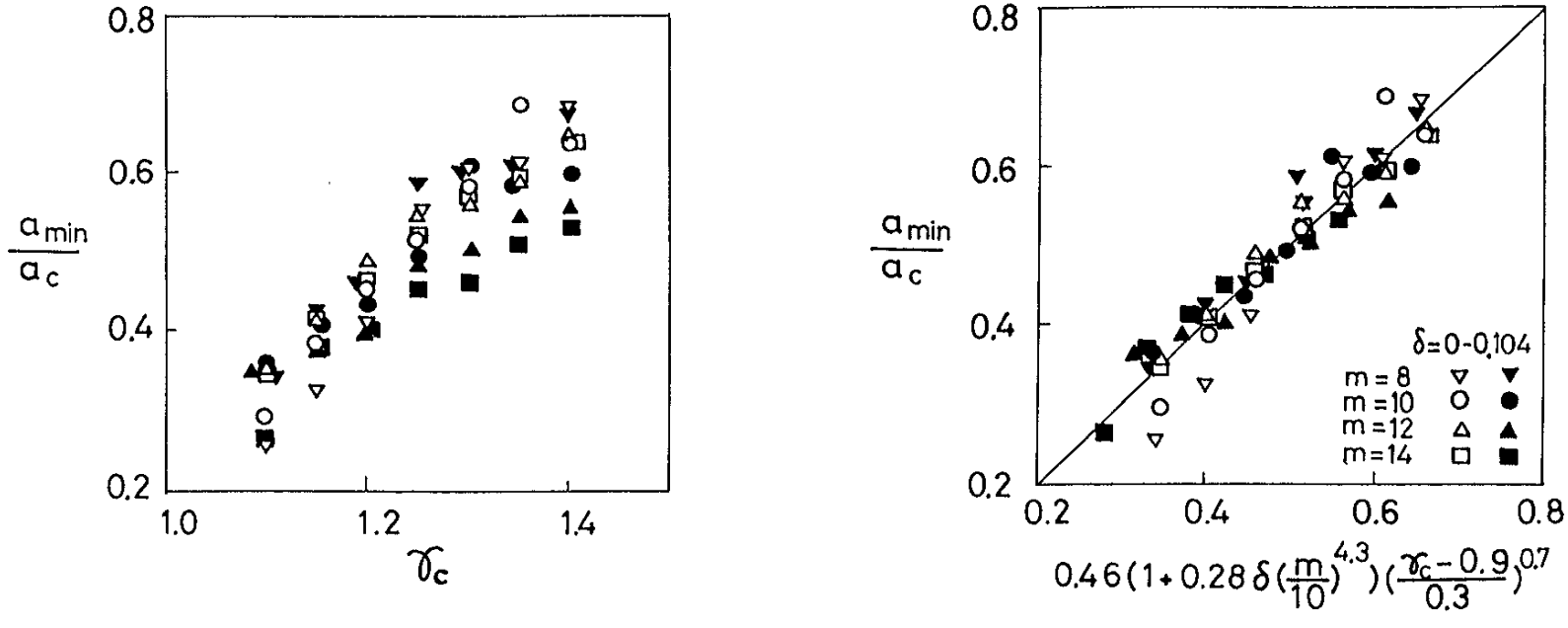
0.8
0.6
0.4
0.2
1.0
1.2
1.4
$\frac{a_{min}}{a_c}$
γ_c
δ=0-0.104
m=8
m=10
m=12
m=14
$0.46(1+0.28\delta(\frac{m}{10})^{4.3})(\frac{\gamma_c-0.9}{0.3})^{0.7}$

Fig.3(b)

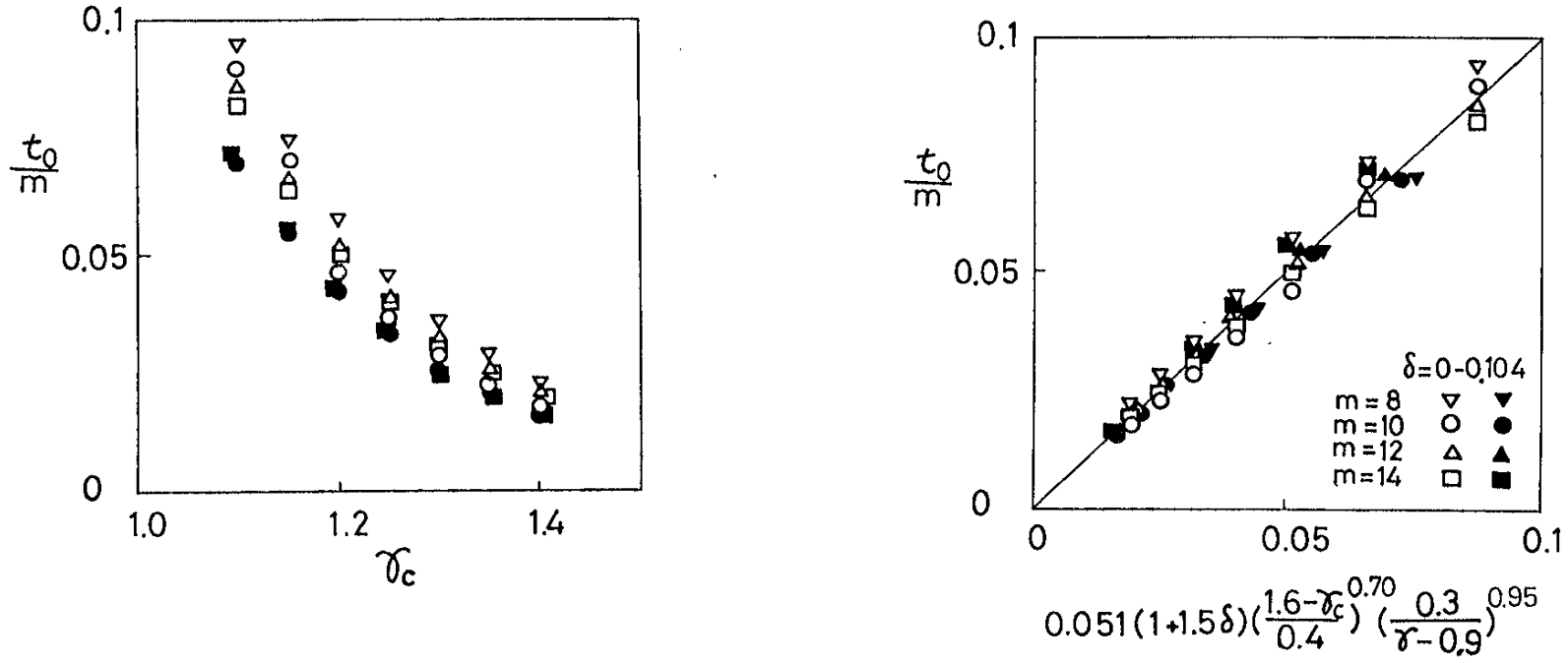
0.1
0.05
0
$\frac{t_0}{m}$
1.0
1.2
1.4
γ_c
0.1
0.05
0
$\frac{t_0}{m}$
δ=0-0.104
m=8
m=10
m=12
m=14
0
0.05
0.1
$0.051(1+1.5\delta)(\frac{1.6-\gamma_c}{0.4})^{0.70}(\frac{0.3}{\gamma-0.9})^{0.95}$

Fig.3(c)

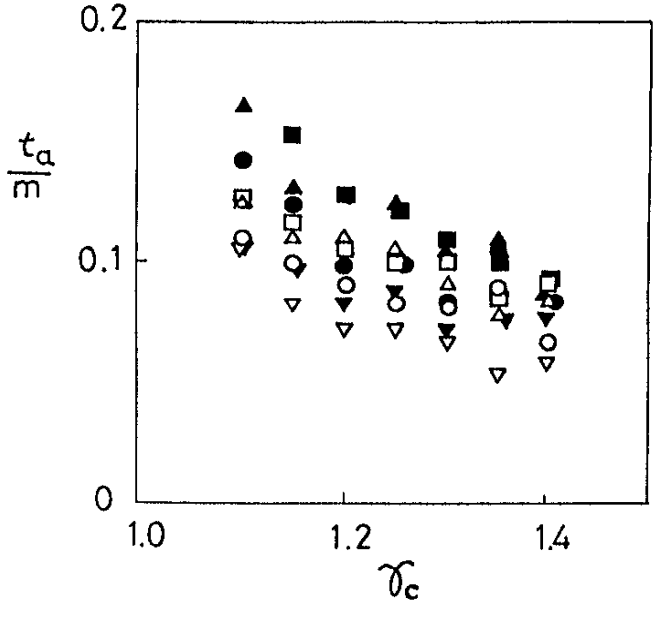
0.2
0.1
0
$\frac{t_a}{m}$
1.0
1.2
1.4
γ_c

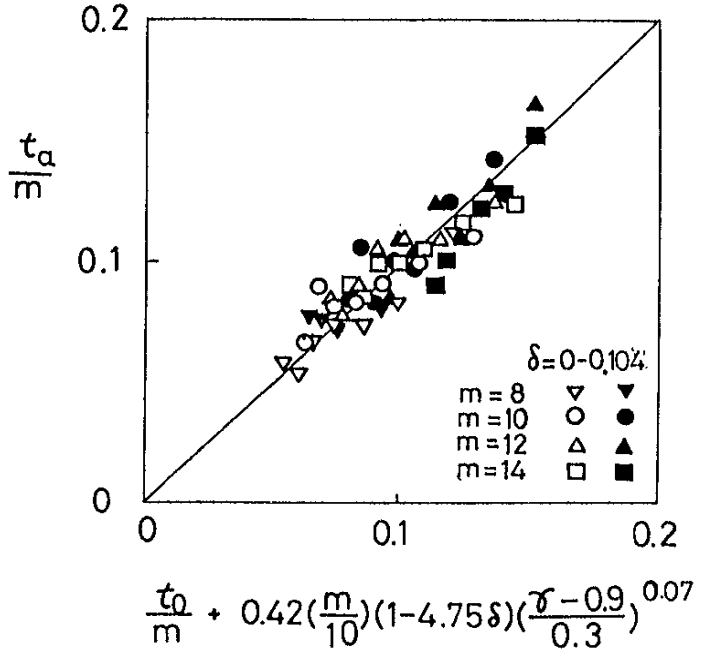
0.2
0.1
0
$\frac{t_a}{m}$
0
0.1
0.2
δ=0-0.104
m = 8
m =10
m =12
m=14
$\frac{t_0}{m} + 0.42(\frac{m}{10})(1-4.75\delta)(\frac{\gamma-0.9}{0.3})^{0.07}$

Fig.3(d)

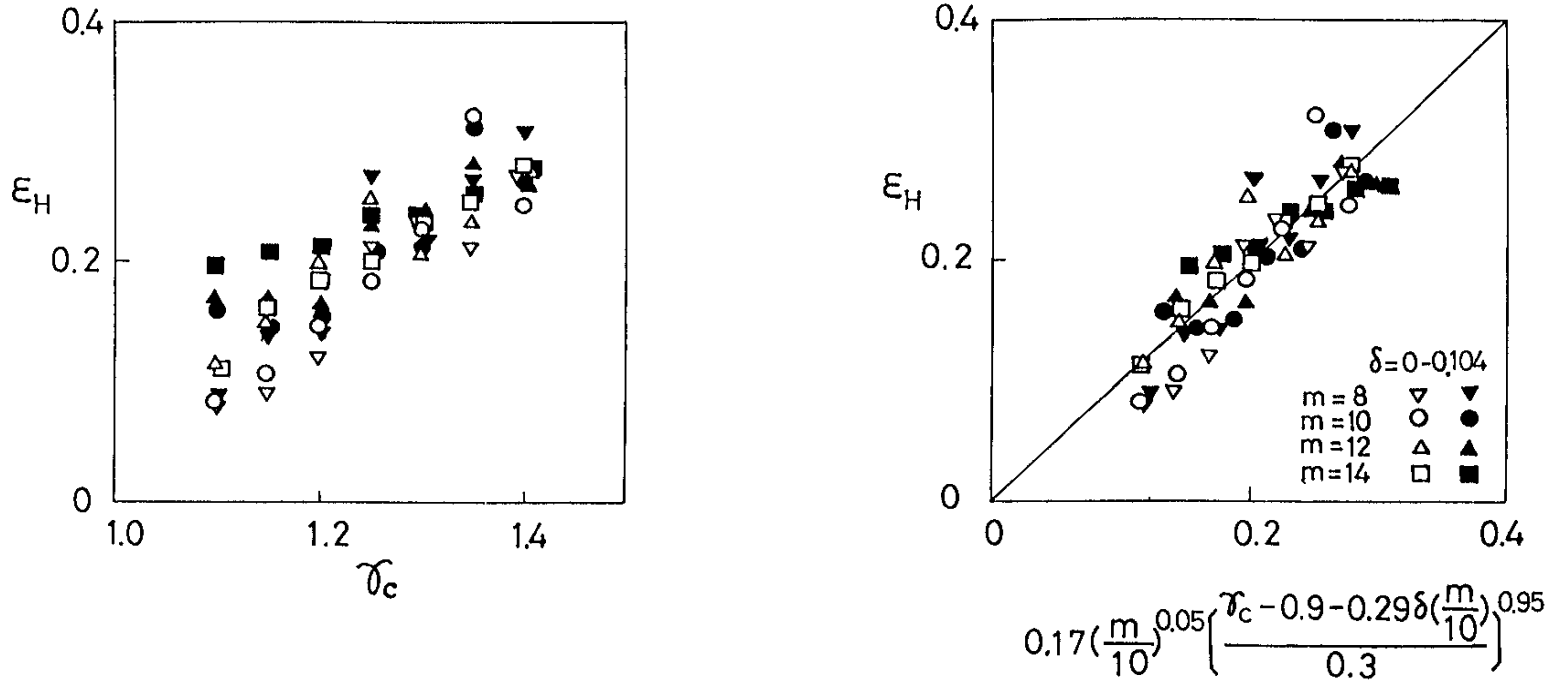
0.4
0.2
0
ε_H
1.0
1.2
1.4
γ_c
0.4
0.2
0
ε_H
0
0.2
0.4
δ=0-0.104
m=8
m=10
m=12
m=14
$0.17\left(\frac{m}{10}\right)^{0.05}\left\{\frac{\gamma_c-0.9-0.29\delta\left(\frac{m}{10}\right)}{0.3}\right\}^{0.95}$

Fig.3(e)

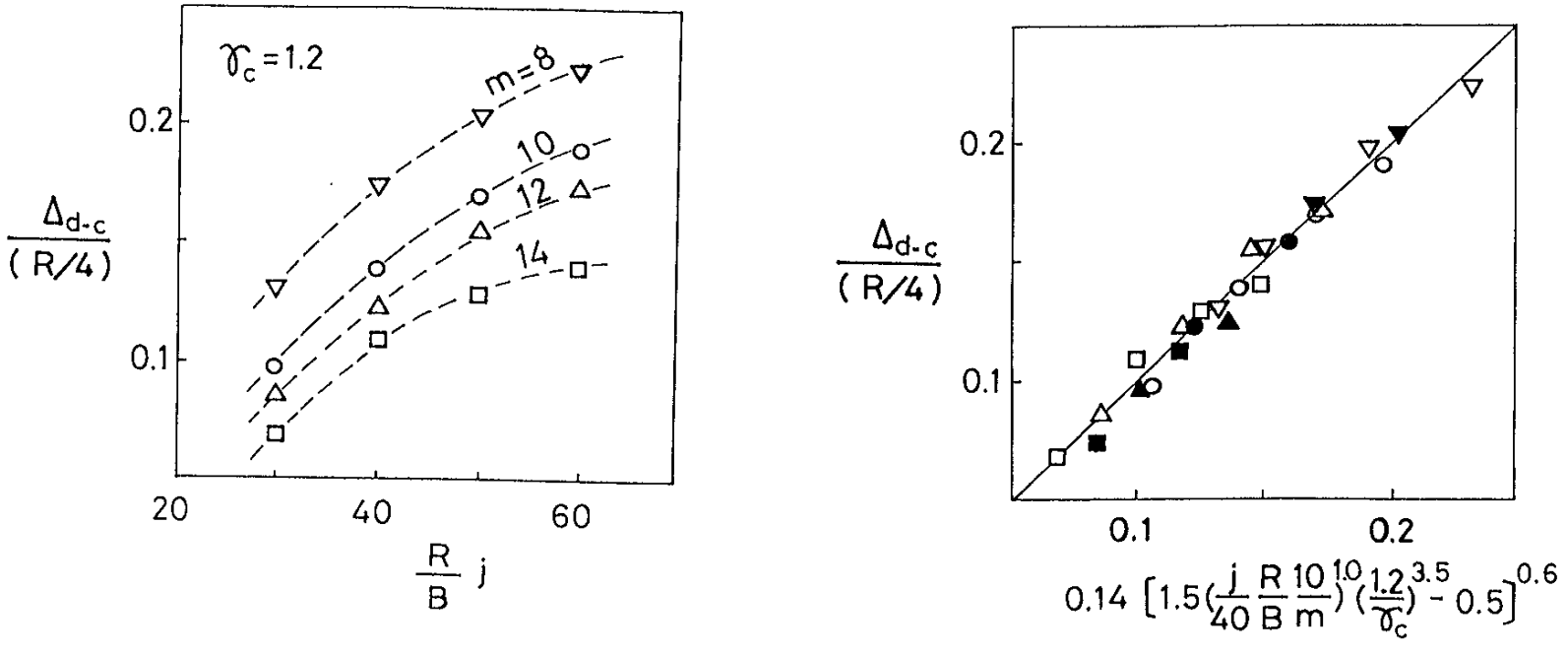
$\gamma_c = 1.2$
m=8
10
12
14
0.2
0.1
20
40
60
$\frac{\Delta_{d-c}}{(R/4)}$
$\frac{R}{B}$ j
$\frac{\Delta_{d-c}}{(R/4)}$
0.2
0.1
0.1
0.2
$0.14\left[1.5\left(\frac{j}{40}\frac{R}{B}\frac{10}{m}^{1.0}\right)\left(\frac{1.2}{\gamma_c}\right)^{3.5} - 0.5\right]^{0.6}$

Fig.4(a)

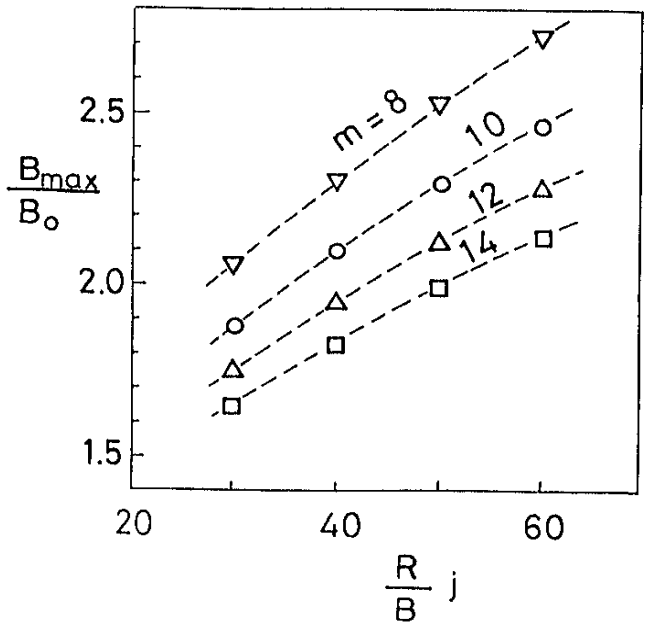
2.5
2.0
1.5
$\frac{B_{max}}{B_o}$
m=8
10
12
14
20
40
60
$\frac{R}{B}$ j

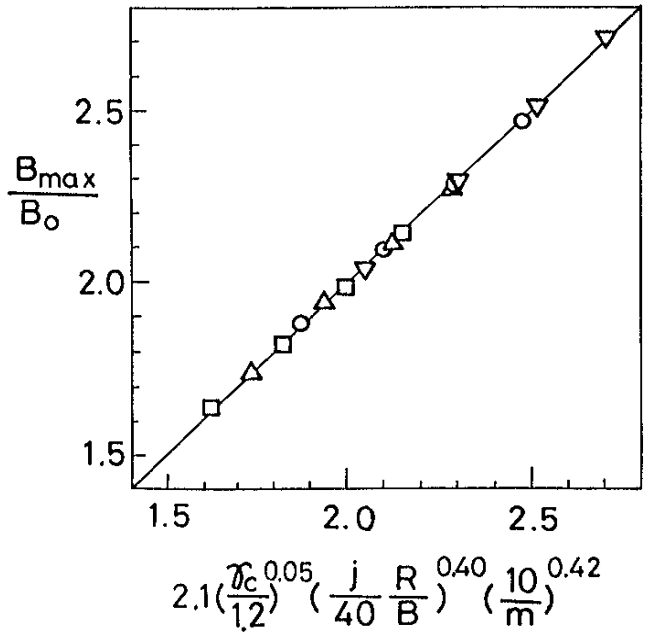
2.5
2.0
1.5
$\frac{B_{max}}{B_o}$
1.5
2.0
2.5
$2.1(\frac{\gamma_c}{1.2})^{0.05}(\frac{j}{40}\frac{R}{B})^{0.40}(\frac{10}{m})^{0.42}$

Fig.4(b)

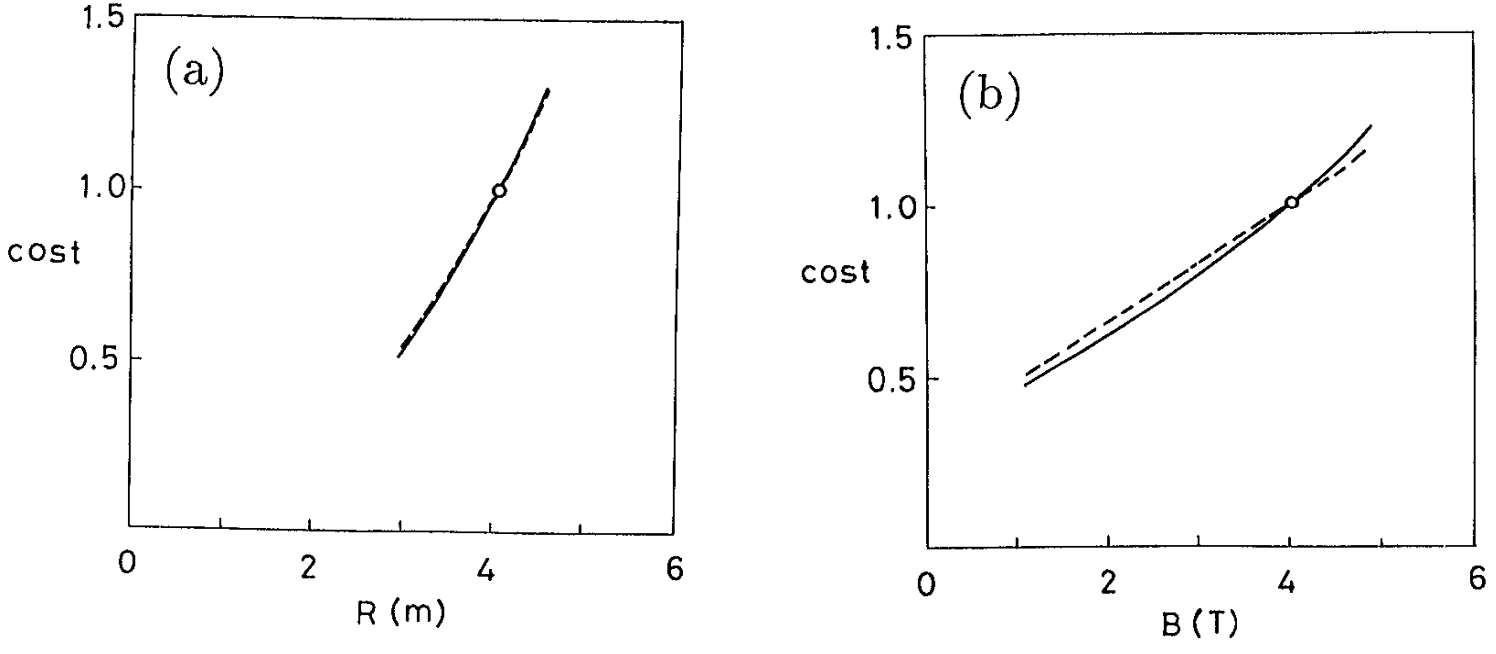

Fig.5

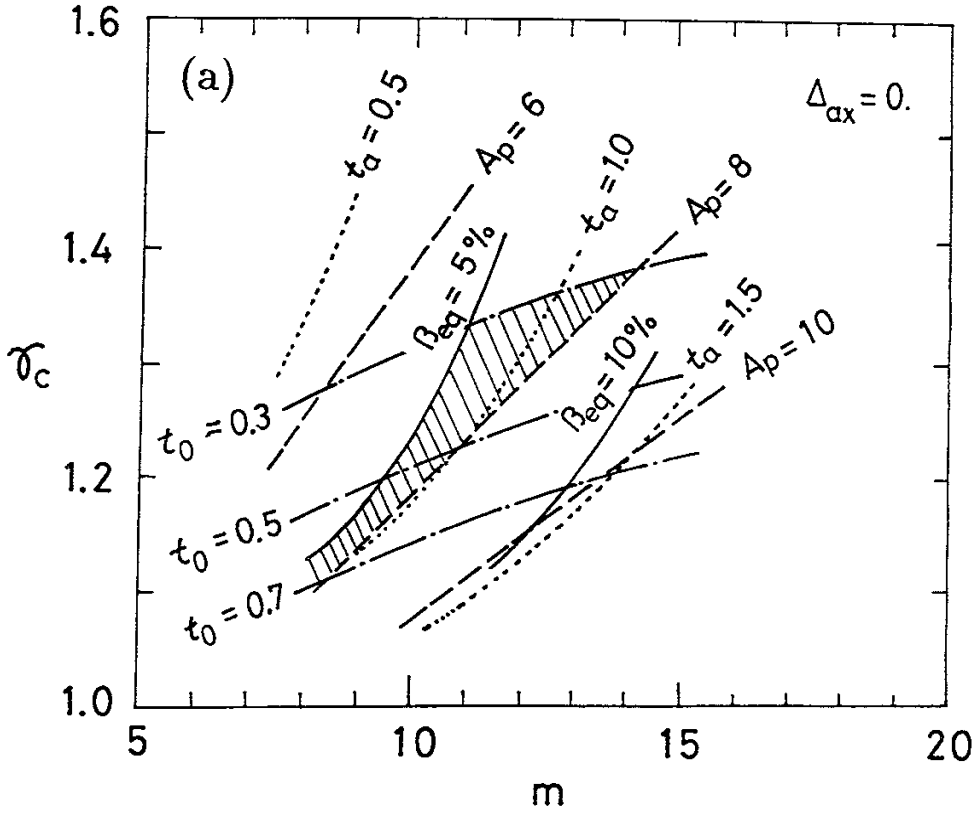
(a)
$\Delta_{ax} = 0.$
$t_a = 0.5$
$A_p = 6$
$t_a = 1.0$
$A_p = 8$
$\beta_{eq} = 5\%$
$\beta_{eq} = 10\%$
$t_a = 1.5$
$A_p = 10$
$t_0 = 0.3$
$t_0 = 0.5$
$t_0 = 0.7$
γ_c
m
1.6
1.4
1.2
1.0
5
10
15
20

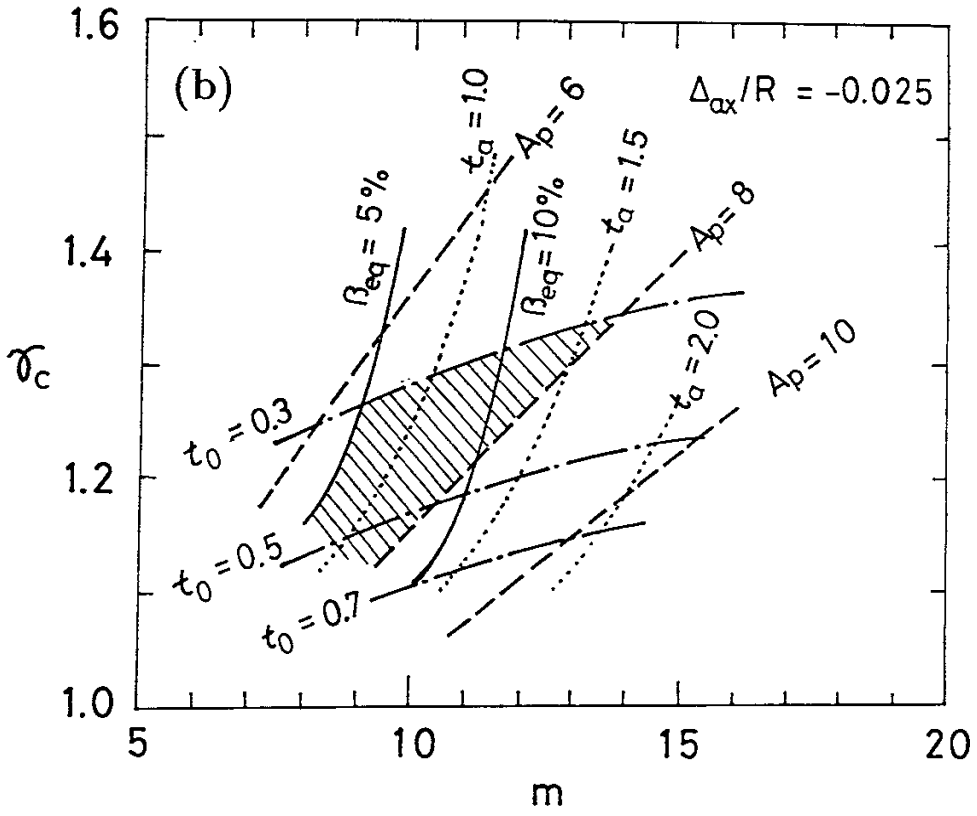
(b)
$\Delta_{ax}/R = -0.025$
$t_a = 1.0$
$A_p = 6$
$t_a = 1.5$
$A_p = 8$
$t_a = 2.0$
$A_p = 10$
$\beta_{eq} = 5\%$
$\beta_{eq} = 10\%$
$t_0 = 0.3$
$t_0 = 0.5$
$t_0 = 0.7$
γ_c
m
1.6
1.4
1.2
1.0
5
10
15
20

Fig.6(a)(b)

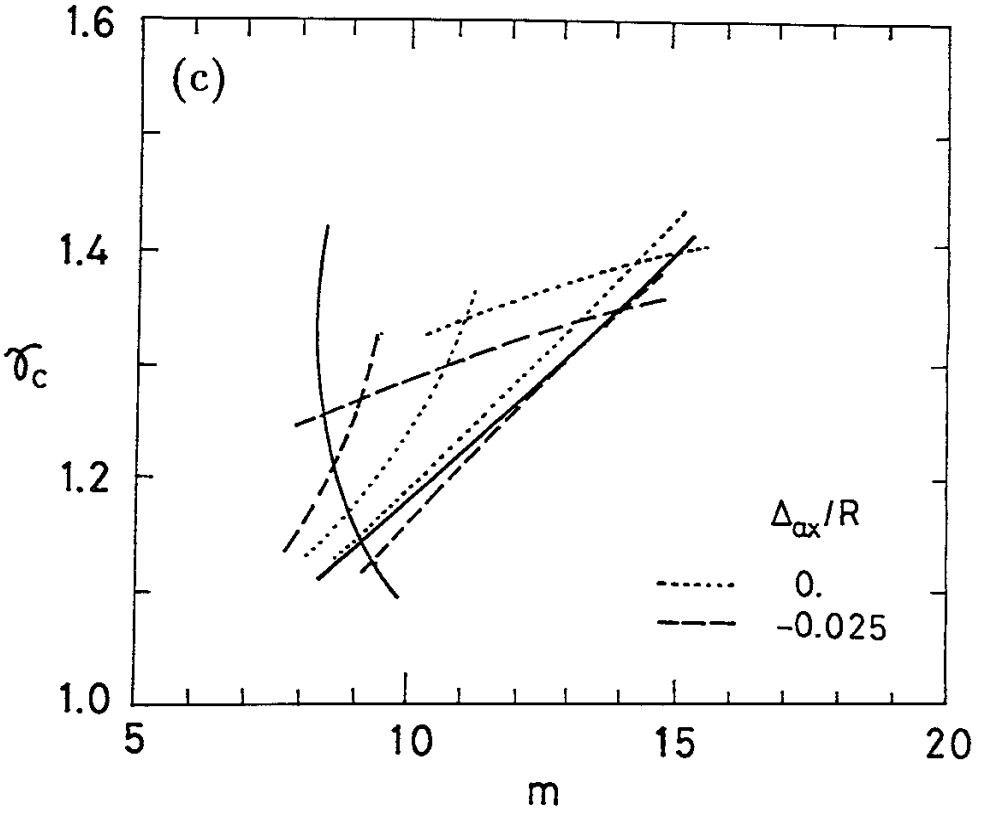

Fig.6(c)

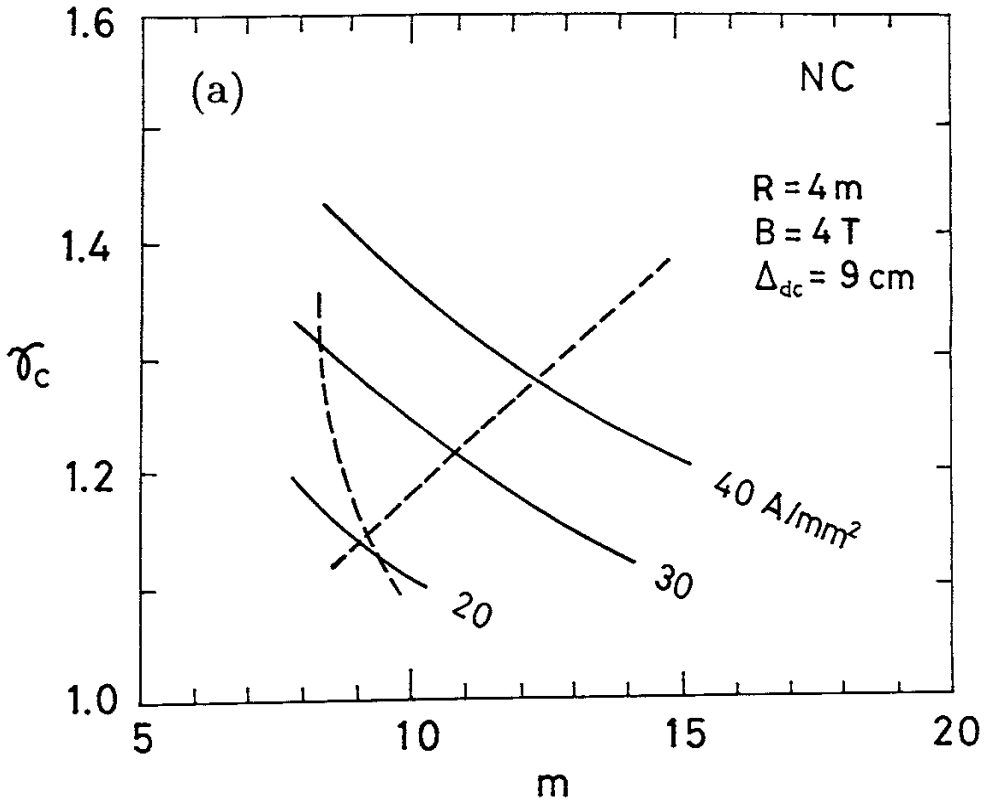
(a)
NC
R = 4 m
B = 4 T
Δdc = 9 cm
40 A/mm²
30
20
γc
1.6
1.4
1.2
1.0
5
10
15
20
m

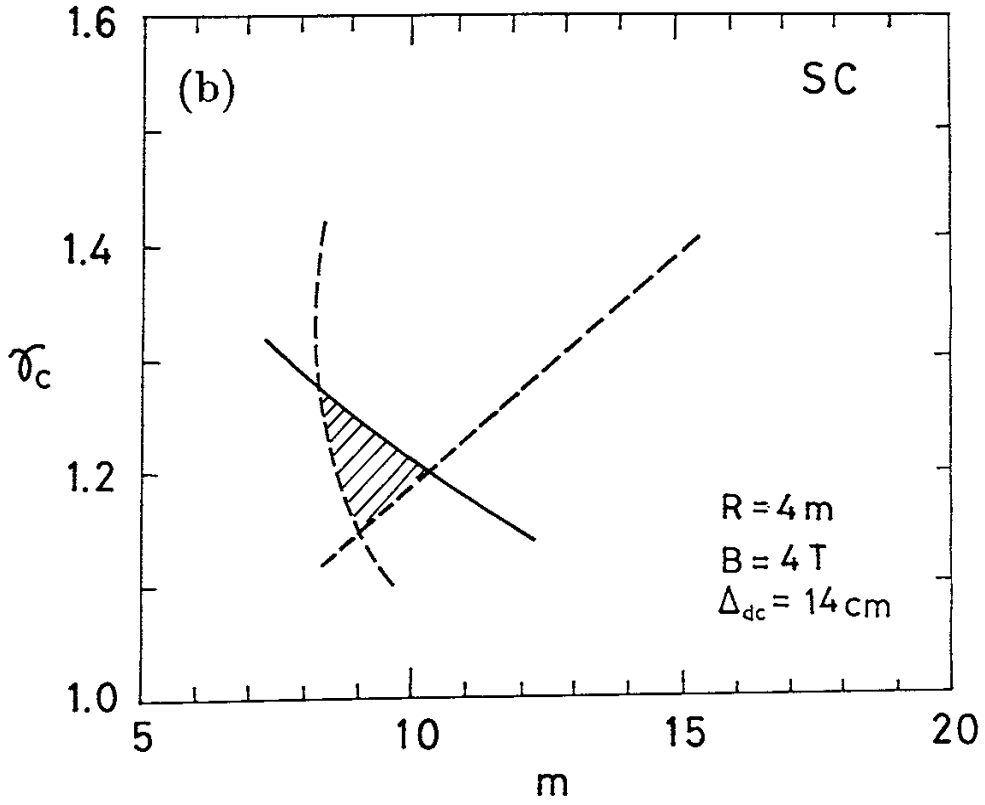
(b)
SC
R = 4 m
B = 4 T
Δdc = 14 cm
γc
1.6
1.4
1.2
1.0
5
10
15
20
m

Fig.7

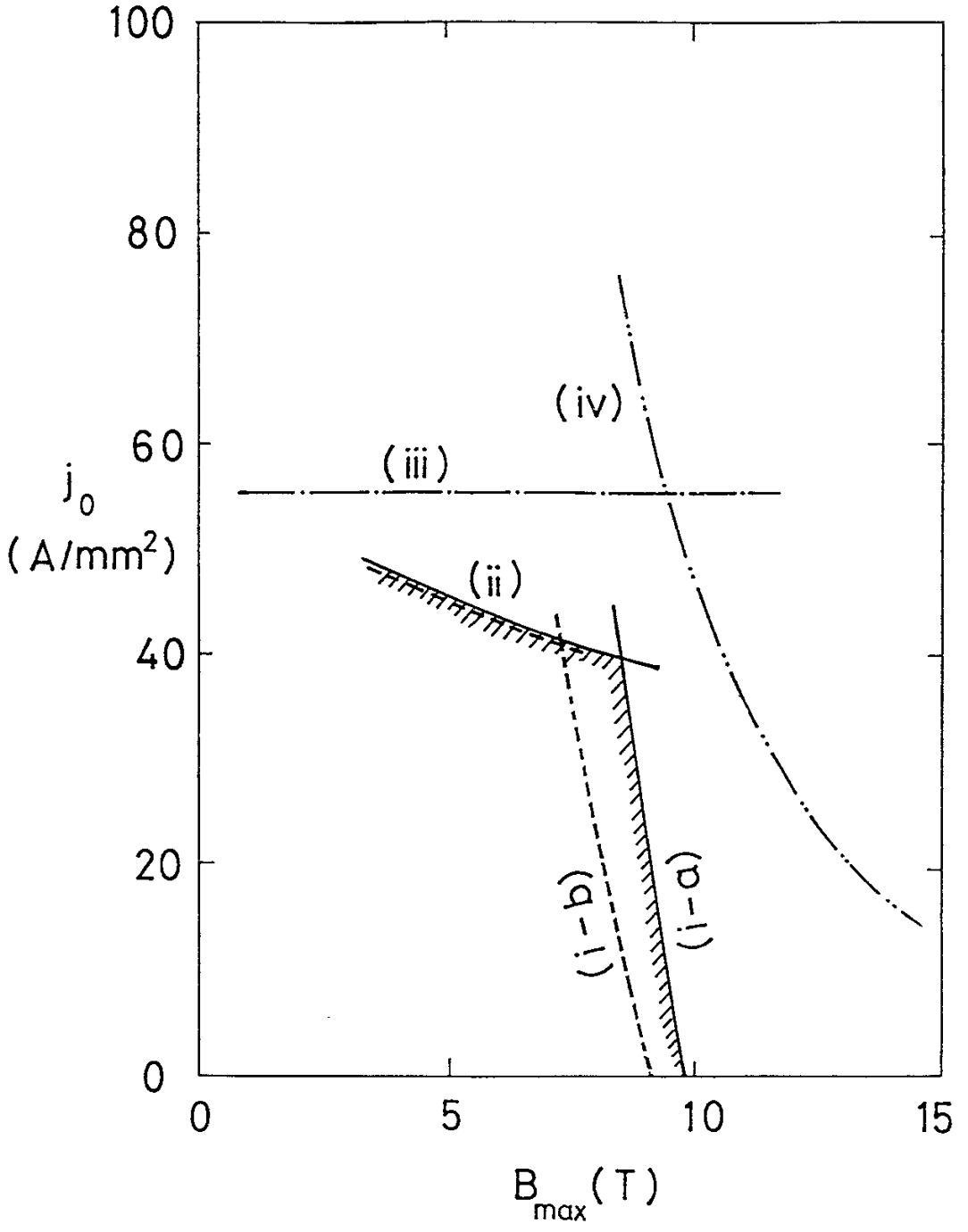

Fig.8

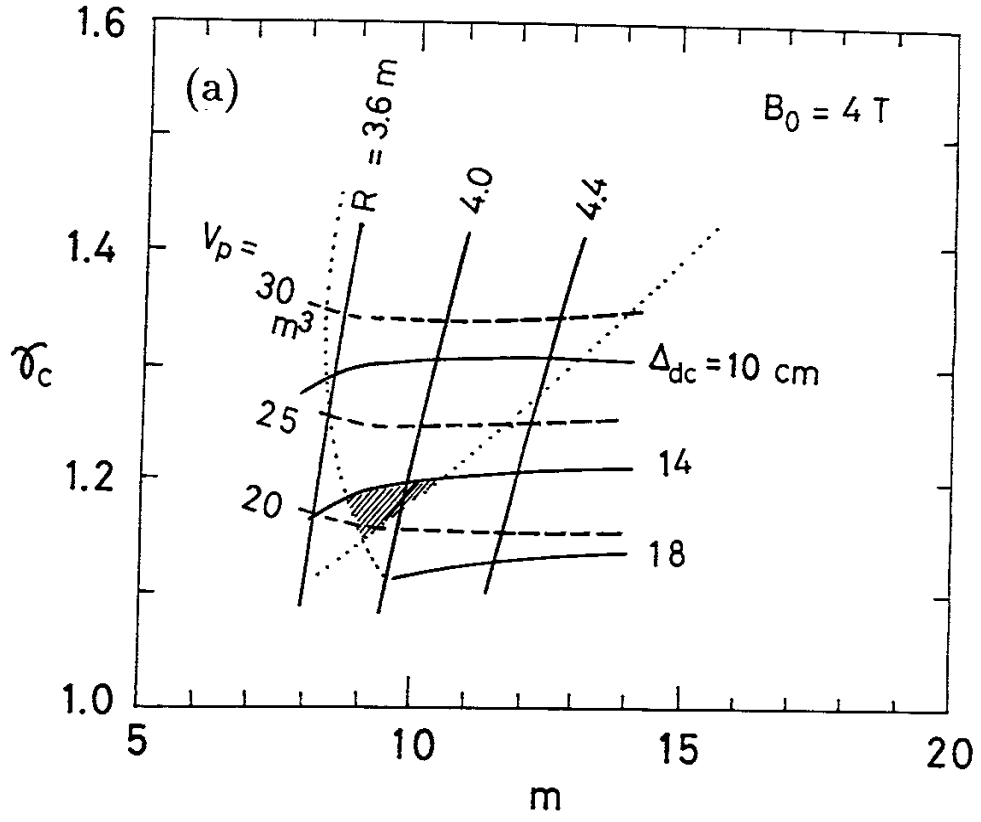
(a)
B_0 = 4 T
R = 3.6 m
4.0
4.4
V_p =
30
31
25
20
Δ_{dc} = 10 cm
14
18
γ_c
1.6
1.4
1.2
1.0
5
10
15
20
m

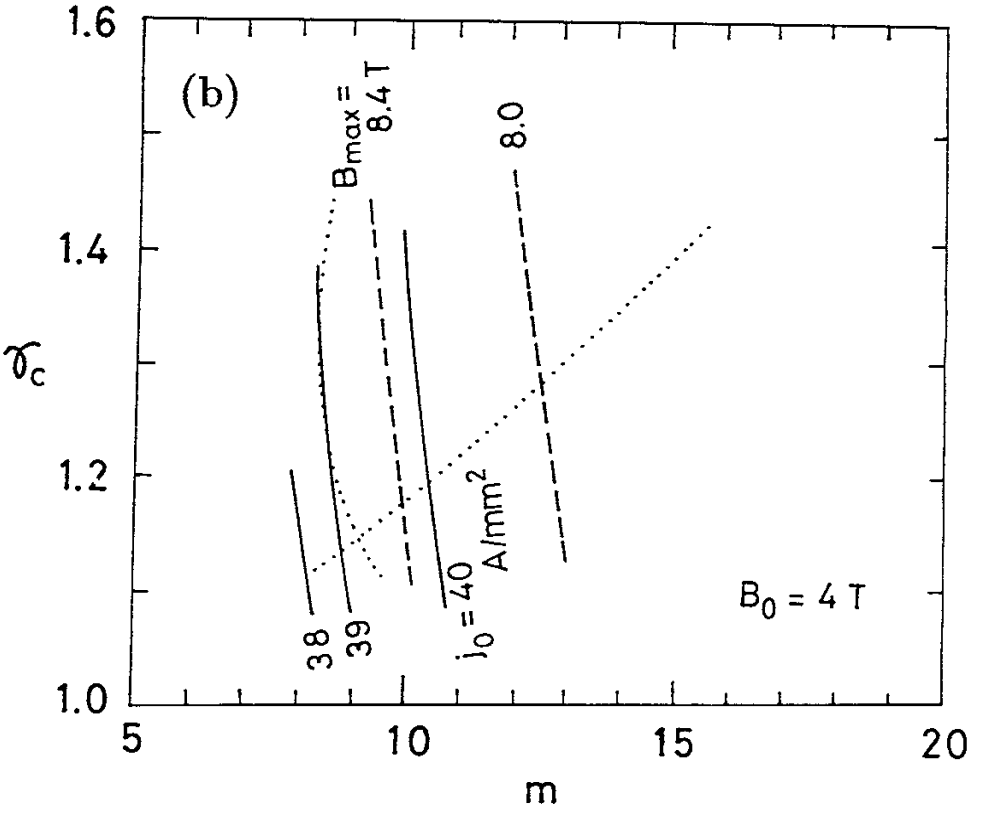
(b)
B_{max} = 8.4 T
8.0
38
39
i_0 = 40 A/mm^2
B_0 = 4 T
γ_c
1.6
1.4
1.2
1.0
5
10
15
20
m

Fig.9(a)(b)

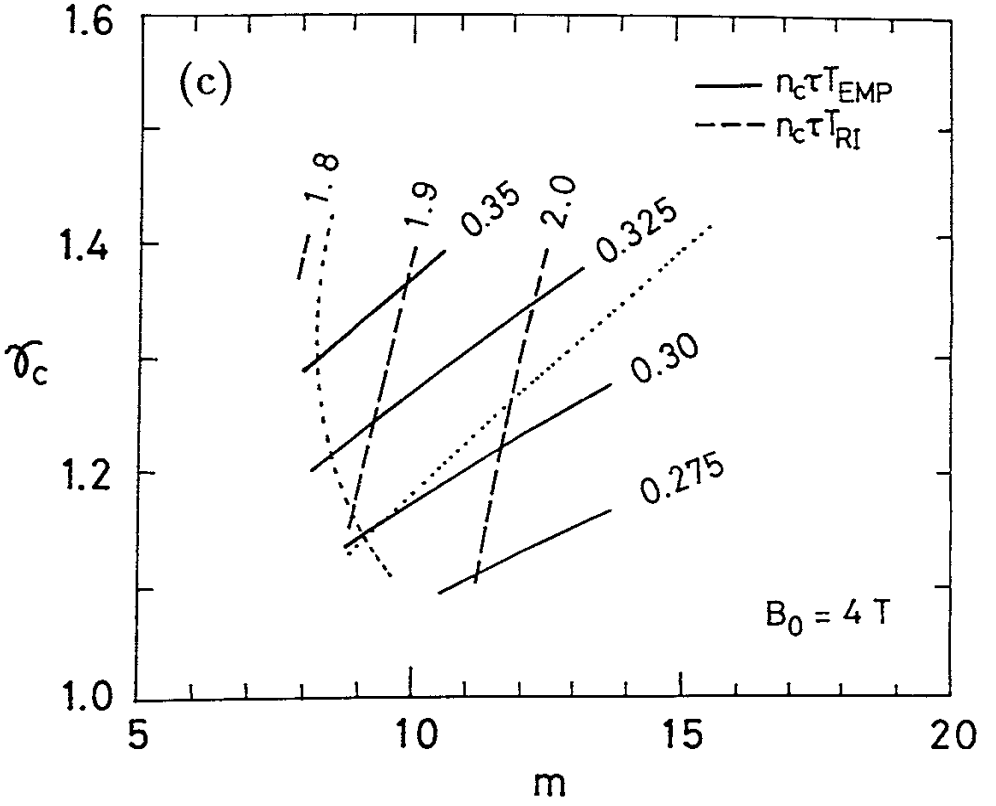
(c)
$n_c\tau T_{EMP}$
$n_c\tau T_{RI}$
1.8
1.9
0.35
2.0
0.325
0.30
0.275
B_0 = 4 T
γ_c
m

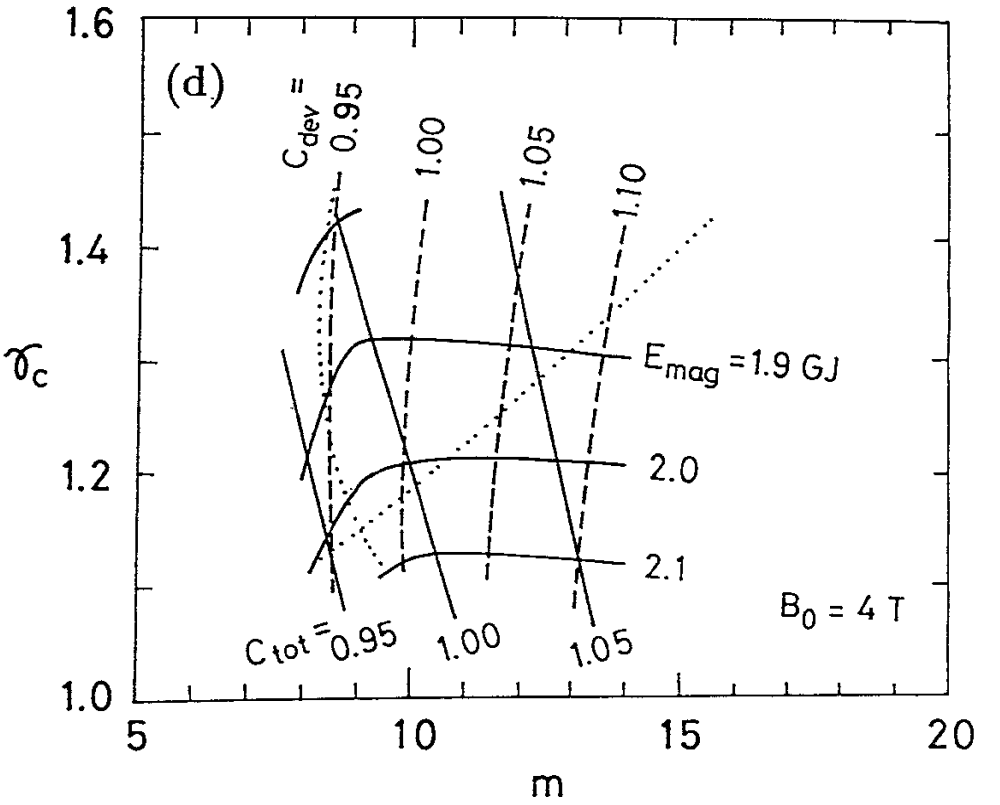
(d)
C_{dev} =
0.95
1.00
1.05
1.10
E_{mag} = 1.9 GJ
2.0
2.1
C_{tot} = 0.95
1.00
1.05
B_0 = 4 T
γ_c
m

Fig.9(c)(d)

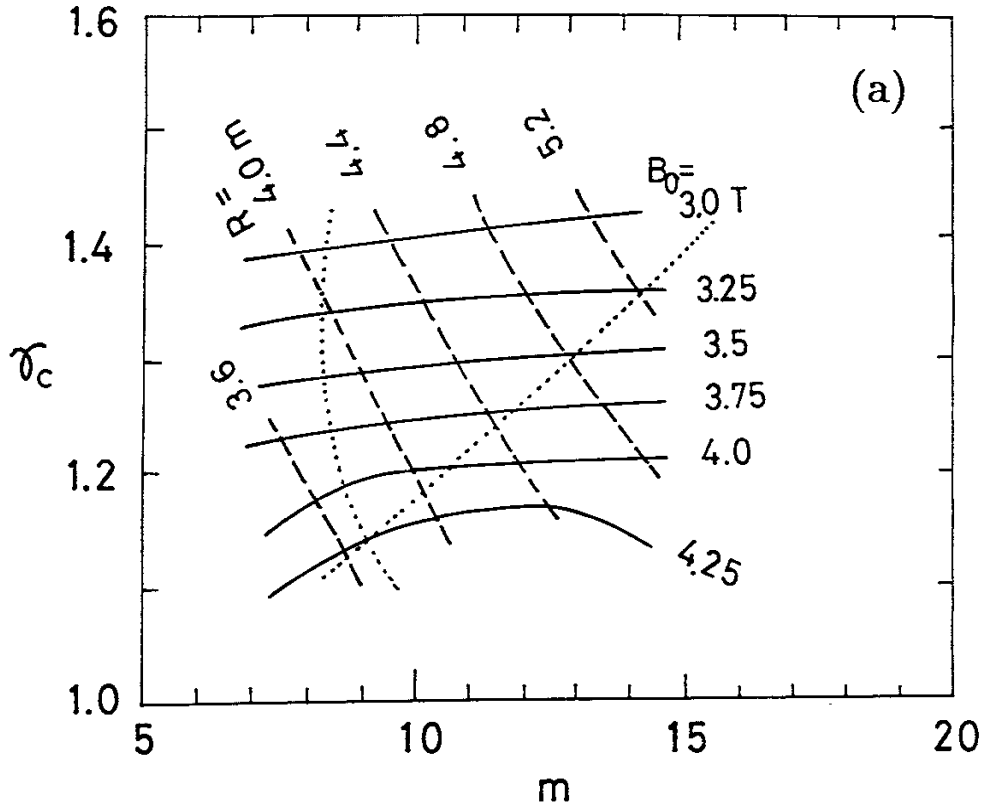
(a)
1.6
1.4
1.2
1.0
γ_c
5
10
15
20
m
R_0 = 4.0 m
4.4
4.8
5.2
B_0=
3.0 T
3.25
3.5
3.75
4.0
4.25

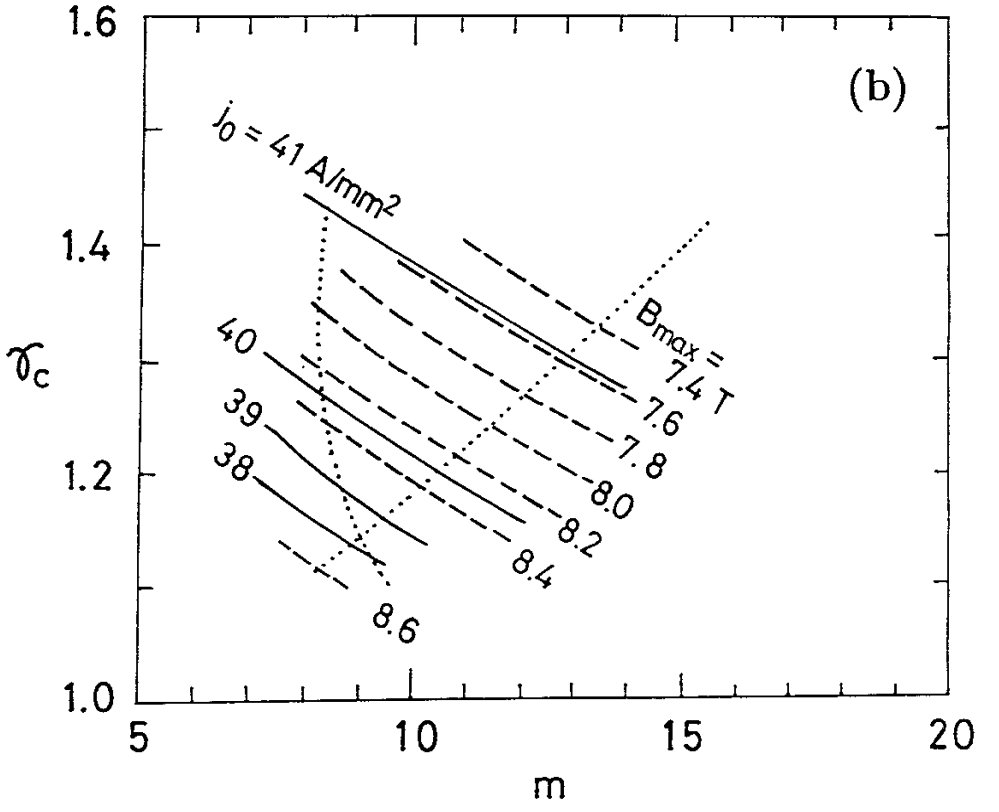
(b)
1.6
1.4
1.2
1.0
γ_c
5
10
15
20
m
j_0 = 41 A/mm²
40
39
38
B_{max} =
7.4 T
7.6
7.8
8.0
8.2
8.4
8.6

Fig.10(a)(b)

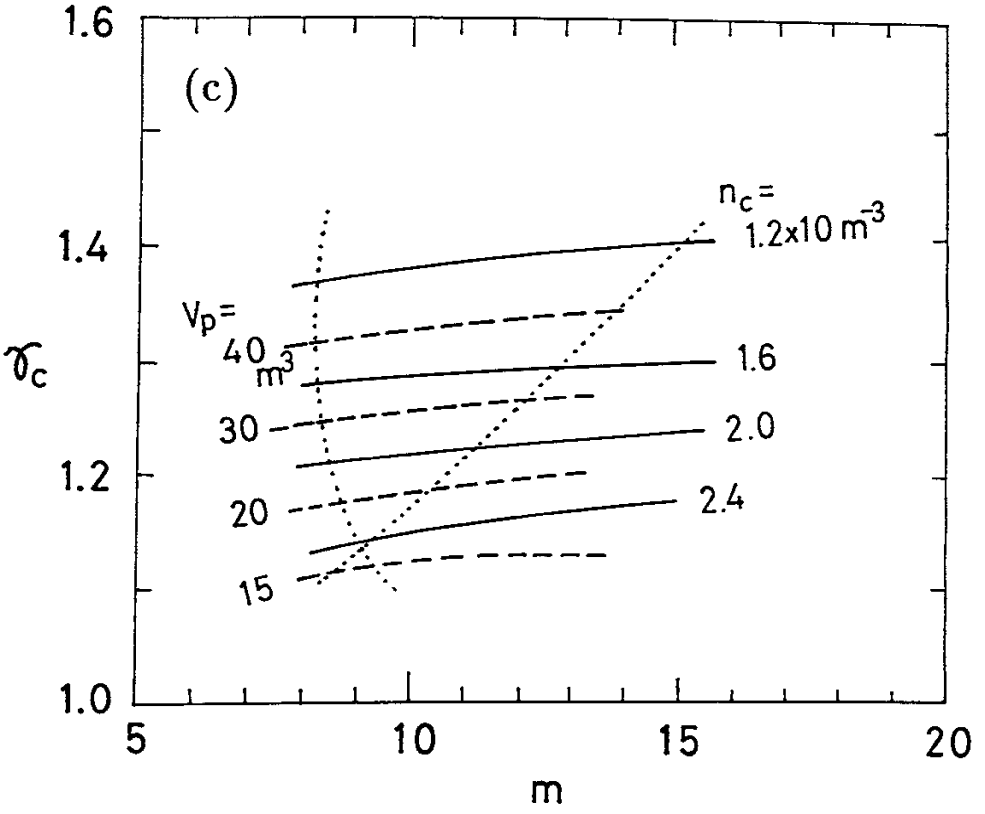
(c)
1.6
1.4
1.2
1.0
γ_c
5
10
15
20
m
n_c = 1.2x10 m^{-3}
V_p = 40 m^3
30
20
15
1.6
2.0
2.4

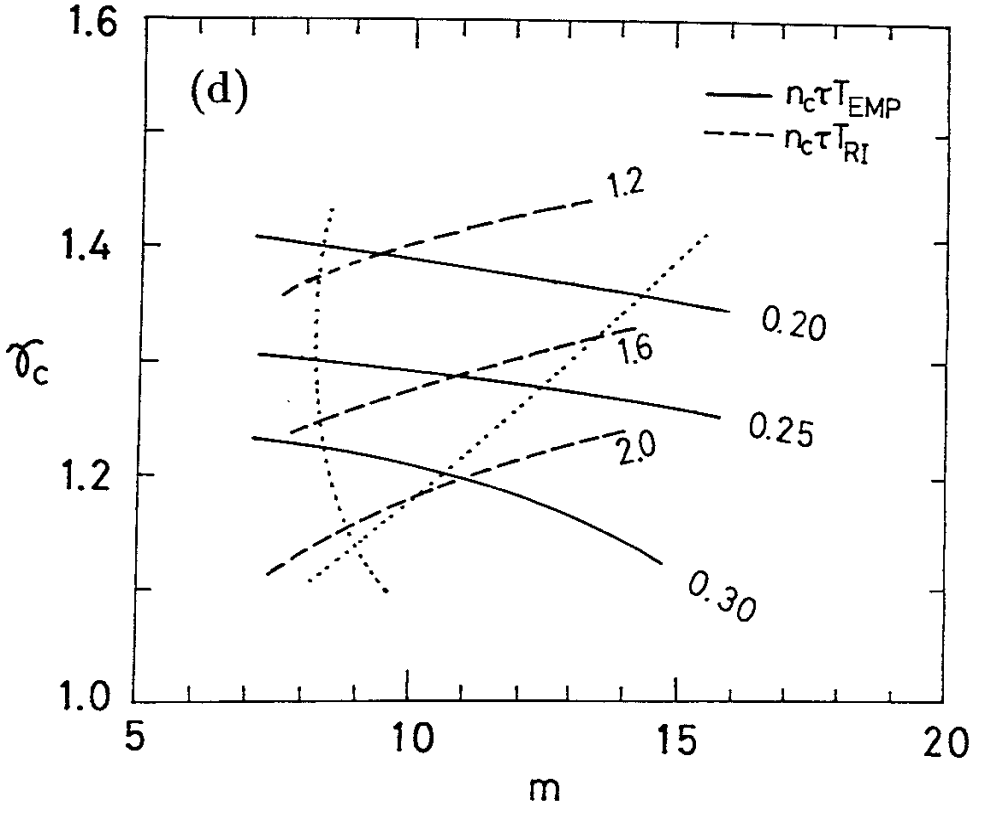
(d)
1.6
1.4
1.2
1.0
γ_c
5
10
15
20
m
$n_c\tau T_{EMP}$
$n_c\tau T_{RI}$
1.2
1.6
2.0
0.20
0.25
0.30

Fig.10(c)(d)

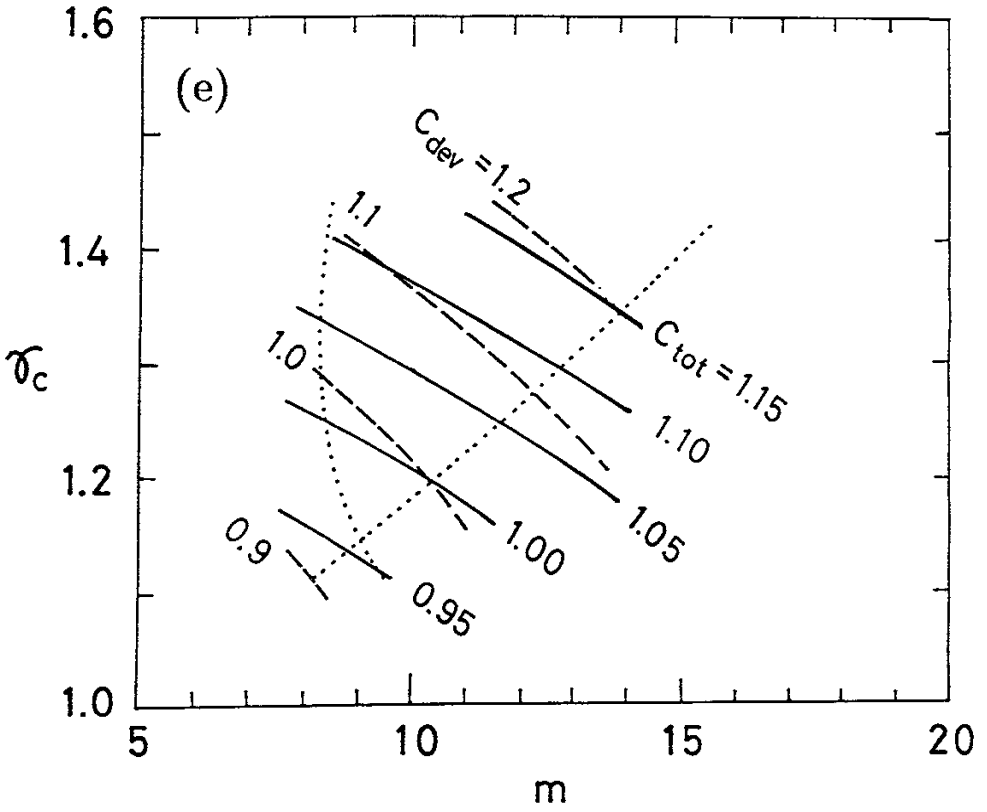
(e)
C_{dev} =1.2
1.1
1.0
0.9
0.95
1.00
1.05
1.10
C_{tot} =1.15
δ_c
1.6
1.4
1.2
1.0
5
10
15
20
m

Fig.10(e)